



# Metallome deregulation and health-related impacts due to long-term exposure to recent volcanic ash deposits: New chemical and isotopic insights

Lucie Sauzéat, Julia Eychenne, Lucia Gurioli, Maud Boyet, David E Jessop, Roberto Moretti, Mélusine Monroe, Hélène Holota, Claude Beaudoin, David Volle

## ► To cite this version:

Lucie Sauzéat, Julia Eychenne, Lucia Gurioli, Maud Boyet, David E Jessop, et al.. Metallome deregulation and health-related impacts due to long-term exposure to recent volcanic ash deposits: New chemical and isotopic insights. *Science of the Total Environment*, inPress, 829, pp.154383. 10.1016/j.scitotenv.2022.154383 . hal-03610668

**HAL Id: hal-03610668**

**<https://uca.hal.science/hal-03610668>**

Submitted on 16 Mar 2022

**HAL** is a multi-disciplinary open access archive for the deposit and dissemination of scientific research documents, whether they are published or not. The documents may come from teaching and research institutions in France or abroad, or from public or private research centers.

L'archive ouverte pluridisciplinaire **HAL**, est destinée au dépôt et à la diffusion de documents scientifiques de niveau recherche, publiés ou non, émanant des établissements d'enseignement et de recherche français ou étrangers, des laboratoires publics ou privés.



Distributed under a Creative Commons Attribution - NonCommercial - NoDerivatives 4.0 International License

# Science of the Total Environment

## Metallome deregulation and health-related impacts due to long-term exposure to recent volcanic ash deposits: new chemical and isotopic insights --Manuscript Draft--

Manuscript Number:	STOTEN-D-21-29496R1
Article Type:	Research Paper
Section/Category:	
Keywords:	volcanic ash deposits, La Soufrière de Guadeloupe volcano, metallome, Cu-Zn isotopes, in-vivo assays
Corresponding Author:	Lucie Sauzeat Laboratoire Magmas et Volcans Aubière Cedex, FRANCE
First Author:	Lucie Sauzeat
Order of Authors:	Lucie Sauzeat Julia Eychenne Lucia Gurioli Maud Boyet David E. Jessop Roberto Moretti Mélusine Monrose Hélène Holota Claude Beaudoin David H. Volle
Abstract:	<p>Volcanic ash exposure can lead to significant health risks. Damage to the respiratory and pulmonary systems are the most evident toxic side effects although the causes of these symptoms remain unclear. Conversely, the effects on other organs remain largely under-explored, limiting our understanding of the long-term volcanic ash-related risk at the whole-body scale. The metallome i.e. metal concentrations and isotopic compositions within the body, is suspected to be affected by volcanic ash exposure, having thus the potential for capturing some specificities of ash toxicity. However, the means by and extent to which the metallome is affected at the entire body scale and how the consequent chemical and isotopic deregulations correlate with pathophysiological dysfunctions are currently poorly understood. Here, we adopt a transdisciplinary approach combining high precision chemical analyses (major and trace element concentrations) and Cu-Zn isotope measurements in seven organs and two biological fluids of isogenic mice (C57BL/6) exposed to eruption products from La Soufrière de Guadeloupe (Eastern Carribean), in tandem with biological parameters including physiological and morphological data. Based on principal component analysis, we show that after one month of exposure to volcanic ash deposits, the mice metallome; originally organ-specific and isotopically-typified, is highly disrupted as shown for example by heavy metal accumulation in testis (e.g., Fe, Zn) and Cu, Zn isotopic divergence in liver, intestine and blood. These metallomic variations are correlated with early testicular defects and might reflect the warning signs of premature (entero)hepatic impairments that may seriously affect fertility and favor the emergence of liver diseases after prolonged exposure. Monitoring the temporal evolution of the Cu and Zn isotope compositions seems to be a promising technique to identify the main biological processes and vital functions that are vulnerable to environmental volcanogenic pollutants although this will require further validation on human subjects.</p>
Response to Reviewers:	Ms. Ref. No.: STOTEN-D-21-29496 Title: Metallome deregulation and health-related impacts due to long-term volcanic ash exposure: new chemical and isotopic insights from la Soufrière de Guadeloupe volcano



## **Highlights**

- Volcanic ash is a major metal-rich contaminant
- Chronic exposure to volcanic ash results into an organ-specific and isotopically-typified metallome deregulation
- Mice metallome deregulations are associated to severe pathophysiological changes
- Quantification of copper and zinc isotopic compositions may appear as an innovative technique to diagnose volcanic-related pathophysiological dysfunctions



# Metallome deregulation and health-related impacts due to long-term exposure to recent volcanic ash deposits: new chemical and isotopic insights

Lucie Sauzéat<sup>1,2</sup>, Julia Eychenne<sup>1,2</sup>, Lucia Gurioli<sup>1,3,4</sup>, Maud Boyet<sup>1</sup>, David Jessop<sup>1,3,4</sup>, Roberto Moretti<sup>3,4</sup>, Mélusine Monroe<sup>2</sup>, Hélène Holota<sup>2</sup>, Claude Beaudoin<sup>2</sup>, David H. Volle<sup>2</sup>

<sup>1</sup> Université Clermont Auvergne, CNRS, IRD, OPGC, Laboratoire Magmas et Volcans, F-63000 Clermont-Ferrand, France

<sup>2</sup> Université Clermont Auvergne, CNRS UMR 6293, Inserm U1103, Génétique, Reproduction et Développement, F-63000 Clermont-Ferrand, France

<sup>3</sup> Université de Paris, Institut de physique du globe de Paris, CNRS UMR 7154, F-75005 Paris, France

<sup>4</sup> Observatoire volcanologique et sismologique de Guadeloupe, Institut de physique du globe de Paris, F-97113 Gourbeyre, France

Corresponding Author: Lucie Sauzéat / mail: [lucie.sauzeat@uca.fr](mailto:lucie.sauzeat@uca.fr)

## Abstract

Volcanic ash exposure can lead to significant health risks. Damage to the respiratory and pulmonary systems are the most evident toxic side effects although the causes of these symptoms remain unclear. Conversely, the effects on other organs remain largely under-explored, limiting our understanding of the long-term volcanic ash-related risk at the whole-body scale. The metallome *i.e.* metal concentrations and isotopic compositions within the body, is suspected to be affected by volcanic ash exposure, having thus the potential for capturing some specificities of ash toxicity. However, the means by and extent to which the metallome is affected at the entire body scale and how the consequent chemical and isotopic deregulations correlate with pathophysiological dysfunctions are currently poorly understood. Here, we adopt a transdisciplinary approach combining high precision chemical analyses (major and trace element concentrations) and Cu-Zn isotope measurements in seven organs and two biological fluids of isogenic mice (C57BL/6) exposed to eruption products from La Soufrière de Guadeloupe (Eastern Caribbean), in tandem with biological parameters including physiological and morphological data. Based on principal component analysis, we show that after one month of exposure to volcanic ash deposits, the mice metallome; originally organ-specific and isotopically-typified, is highly disrupted as shown for example by heavy metal accumulation in testis (*e.g.*, Fe, Zn) and Cu, Zn isotopic divergence in liver, intestine and blood. These metallomic variations are correlated with early testicular defects and might reflect the warning signs of premature (entero)hepatic impairments that may seriously affect fertility and favor the emergence of liver diseases after prolonged exposure. Monitoring the temporal evolution of the Cu and Zn isotope compositions seems to be a promising technique to identify the main biological processes and vital functions that are vulnerable to environmental volcanogenic pollutants although this will require further validation on human subjects.

**Keywords:** volcanic ash deposits, La Soufrière de Guadeloupe volcano, metallome, Cu-Zn isotopes, *in-vivo* assays

## 1. Introduction

Covering approximatively 124 million hectares of the world's land surface<sup>1</sup>, volcanic ash soils are home to more than 8 million people<sup>2</sup>. By definition, volcanic ash soils designate soils formed from volcanoclastic materials including ash<sup>3</sup> (defined as small fragments of quenched magma and eroded substratum smaller than 2 mm in diameter). Such soils are regularly formed, given that every month, active volcanoes release more than a million cubic meters of volcanic ash into Earth's atmosphere<sup>4</sup>. Upon injection, ash undergoes several physicochemical processes including interactions with gas, aerosols and anthropogenic pollutants compounds that may affect its surface composition and reactivity<sup>5,6</sup>. These volcanic particles are then

deposited within minutes to years on the ground followed by wind- and water-driven erosion, long-term stabilization, consolidation and finally pedogenesis processes accounting for volcanic soil formation<sup>3,5</sup>. The intensity of wind erosion and the subsequent resuspension of deposited volcanic ash, which can be a dominant feature of a post-eruptive landscape<sup>5</sup>, coupled with intense human activities may result in long-term human exposure to these soil particles. Particle absorption can occur by several exposure pathways, including inhalation as well as oral and dermal uptake and thus represent a major health issue. So far, only a few biological studies using animal models focused on the impact of acute exposure to ultra-fine volcanic particles (<10 µm) either by inhalation or intratracheal injection over short periods of time<sup>7,8,9</sup>. These studies demonstrate that short-term intense volcanic ash exposure induces adverse effects on the respiratory tracts<sup>7,9</sup>. Biological studies on pulmonary cell models also point towards acute inflammatory reaction<sup>10–12</sup>. In parallel, several epidemiological studies show higher incidences of respiratory diseases such as chronic bronchitis<sup>13</sup> in some volcanic areas affected by volcanic ash fallout, as well as other pathologies like multiple sclerosis<sup>14</sup>, thyroid<sup>15</sup> and gastrointestinal cancers<sup>16</sup> in populations living daily in a volcanic environment. This may suggest a more global and longer-term relationship, likely resulting from multiple uptake routes not limited to inhalation, between volcanogenic contaminants exposure, including volcanic ash, and health impairments, although this remains to be proven. Another important point relies on the toxicity parameters, as the nature and the intensity of the symptoms may depend on the physico-chemical properties of the volcanic particles. Studies have shown that cristobalite, a crystalline silica phase, was a main component of volcanic ash inducing inflammation<sup>11</sup>; crystalline silica being also known for triggering silicosis<sup>17</sup>, a type of pulmonary fibrosis. However, crystalline silica is not the only toxic compound present in volcanic deposits as metals, such as copper (Cu), zinc (Zn) and iron (Fe), may also contribute to volcanic particles' toxicity. So far, only few studies have focused on these trace elements<sup>15,18</sup>, with a specific focus on chemical concentrations to the detriment of stable isotopic compositions, but none of them has never quantified the whole-body metallome deregulations at the entire body-scale following chronic exposure. The term metallome refers here to the entirety of metal- and metalloid species present in a biological system, defined as to their identity (e.g. isotopic form) and/or quantity (concentration) (for a complete definition see Lobinski et al.<sup>19</sup>). Recently recognized as very promising tools in the medical field, stable metal isotope analyses have contributed to the development of new research perspectives to better understand the complexity, causes and underlying mechanisms of aging<sup>20,21</sup> and many severe diseases such as cancers<sup>22</sup> and neurodegenerative disorders<sup>23</sup>.

Firstly, the present study aims at elucidating whether long-term exposure to recently ground-deposited volcanic ash (a proxy of premature volcanic soils i.e. early stage of pedogenesis) by various and simultaneous exposure routes (inhalation, oral and dermal) contribute to widespread metallome deregulations related to severe pathological disorders at the entire body-scale. Secondly, this project focus at determining to what extent stable isotopes may help to better characterize the toxic and potentially carcinogenic effect of ash-derived metals in a volcanically active area. We report on the metallome of seven organs and two body fluids (blood and urine) in tandem with a series of physio-, immuno- and morphological data collected on mice exposed to bulk "volcanic ash-made" from La Soufrière de Guadeloupe volcano (hereby referred to as "La Soufrière"). La Soufrière is an explosive-type active volcano located in the Lesser Antilles arc that has experienced many magmatic and phreatic eruptions in the past. The last 1976-1977 phreatic eruptive crisis was characterized by important steam blasts that gave rise to particle and sometimes block-charged plumes resulting in the deposition of 10<sup>6</sup> m<sup>3</sup> of volcanic ash and blocks on the ground<sup>24</sup>. After that, a regular decrease in the activity of La Soufrière was observed until the beginning of the 1990s. Since 1992, the volcanic and seismic activity shows a gradual increase that reached a record level on 27 April 2018 with the largest volcano-tectonic earthquake (M<sub>L</sub> 4.1) associated to an intense hydrothermal and fumarolic activity<sup>25</sup>. This event, regarded as a failed phreatic eruption<sup>25</sup>, marked a significant change of the volcano regime that may foreshadow the onset of an upcoming series of phreatic and magmatic eruptions, resulting in large volcanic ash fallout. The current level of volcanic activity includes regular swarms of volcano-tectonic earthquakes, active degassing from a

number of high-flux fumarole vents, and a spreading and intensification of ground thermal anomalies at the summit<sup>26,27</sup>. These signs indicate that the ongoing unrest may escalate towards more explosive activity (either phreatic or magmatic) in the future, meaning that studies on the health impacts of volcanic emissions at La Soufrière are highly worthwhile due to the major population zones (~20 000 people within 10 km of the volcano). Furthermore, as La Soufrière is a close analogue for numerous other andesitic to dacitic “arc” volcanoes (i.e. with a similar rock composition<sup>28,29</sup>) worldwide, such studies are of great importance for our understanding of the health impacts of volcanoes on human and other organisms.

## **2. Materials and methods**

### **2.1. Geological field sampling and sample preparation**

Because recently ground-deposited fresh volcanic ash was not available at La Soufrière, a laboratory-crushed volcanic ash was produced. The aim was to simulate, within uncertainties of experimental protocols, a proxy of premature volcanic soils. Volcanic ash can be generated by the fragmentation of rocks present on the volcanic edifice, especially during dome-collapse explosive eruptions. We thus collected four volcanic blocks (S01-S04) from the most recent lava dome (emplaced during the AD 1530 eruption<sup>30</sup>) at two active sites that are the “Tarissan” and the “Cratère Sud” (Figure 1; see Supp. Table 1 for GPS coordinates). These blocks, exhibiting a pronounced surface alteration but well-preserved internal facies (Supp. Figure 1a), were crushed using a Jaw crusher BB 250 (Retsh Company) heavy-metal free steel grinding tool before being separated in different size fractions at half-phi size intervals (where  $\Phi = -\log_2[\text{particle diameter in mm}]$ ), using stainless-steel sieves (SAULAS brand). Particle grainsize analyses were performed on the size fraction finer than 63 $\mu\text{m}$  using the laser diffraction technique (Malvern Mastersizer®). Defined amounts of each fraction were then mixed together to reproduce a realistic particle size distribution for volcanic ash (i.e., mirroring the average grain size of volcanic particles commonly produced by explosive eruptions<sup>31</sup>), with a median grainsize of about 100  $\mu\text{m}$  (3.5 $\Phi$ ) (Supp. Figure 1b). The fraction above 2 mm (-1 $\Phi$ ) was excluded, volcanic ash being defined as volcanic particles <2 mm (<-1 $\Phi$ ) in size.

### **2.2. Mice *in-vivo* assays**

#### **2.2.1. Ethics statement**

In this study, all the animal experiments comply with the ARRIVE and the EU Directive 2010/63 guidelines and were conducted in accordance with the current regulations and standards approved by the Animal Care Committee (APAFIS #33604).

#### **2.2.2. Exposure protocol**

Because of their genetic, physiological and metallomic regulation processes homologies with humans<sup>32,33</sup>, mice have long served as models of human biology and provide, so far, the foremost mammalian model for studying human diseases and more broadly human health. Male C57BL/6 mice (5-month-old) were purchased from Charles River Laboratories and maintained under 12-hour light/dark cycles, in controlled temperature, pressure and atmospheric (22°C, humidity <50%) cages (500 cm<sup>2</sup> EasyCage® - Allentown; three mice per cage). To mimic chronic exposure, mice were exposed to volcanic ash over a month. C57BL/6 mice have a median lifespan ranging between 27 to 29 months, equivalent to a human lifespan of 80-84 years. By analogy, one month on a mouse scale will thus correspond to about 3 years of persistent exposure for a human. All the cages were previously filled with 100 g of corn cob litter (NestPak®) for the control group (n=6) or a mixture of corn cob litter (NestPak®) and volcanic ash (200 g of litter for 100 g of ash) for the exposed group (n=6). To ensure breathable air, cages were supported by EcoFlo™ ventilated rack mounted blowers with a total air volume renewed 50 times per hour. Over the time exposure, mice had *ad libitum* access to food (Teklad Global Rodent Diet®, Envigo+++ ) and water. The chemical composition of the diet is given in Supp. Table 2. Body weight as well as food and water intake were measured three times per week to establish growth curves and estimate daily food (g/day/mouse) and water (mL/day/mouse) consumption (Supp. Table 3 and Supp. Figure 2).

## 2.3. Biological samples collection, preparation and measurements

### 2.3.1. Sample collection & preparation

After one month of exposure, urine was first collected in acid-cleaned Eppendorf tubes®. To ensure sufficient volume for precise chemical and isotopic measurements, the urine of the mice present in the same cage were pooled. All mice were then sacrificed by decapitation and organ dissection was performed with acid-clean scissors and vinyl gloves to ensure minimal metal exogenous contamination. Chemical (e.g., pentobarbital) and inhalant gas (e.g., isoflurane, CO<sub>2</sub>) anesthetics, commonly used to euthanize the mice as well as some type of gloves may contain elevated amounts of metals than can significantly bias the chemical and isotopic results<sup>34</sup>. Decapitation is thus the most suitable alternative technique with regard to its lowest chemical contamination effect. Like for urine, blood was collected into acid-clean Eppendorf tubes®, taking care not to use plastic syringes and traditional collection tubes like heparinized or rubber-stoppered evacuated tubes that may give rise to significant and artificial increase of blood, plasma and serum metal contents up to 250%<sup>35,36</sup>. For the organs, we collected liver, brain, lung, kidney, intestine, testis and heart. Each of them was then weighed (Supp. Table 4). Entire organ for brain, heart, intestine and half organ for liver, kidney, testis and lung were then freeze-dried for 48h (Christ Alpha<sup>TM</sup> Freeze dryer 1-2 LD+). All samples were stored at -80°C until further chemical processing.

### 2.3.2. Histology & Sperm counts

For liver, kidney, testis and lung, the remaining part was paraformaldehyde (PFA)-fixed for 48h and embedded in paraffin. Five µm thick sections were then prepared and stained with Hematoxylin/Eosin (HE) and Masson's Trichrome (TM) for histological analysis using a Zeiss Axioscan Microscope Slide Scanner. For testes, epididymal sperm counts and quantification of the epithelium thickness ( $R_{epi}$ ), defined as the ratio between the total ( $D_t$ ) and the inner diameter ( $D_i$ ) of the seminiferous tubules, were also performed. All data are reported in Supp. Tables 5 and 6 respectively. To avoid any analytical bias, all these analyses were performed only in rounded tubules ( $n > 20$  per sample). For sperm counts, the tail and the head of the epididymis were disrupted and placed in phosphate buffered saline (PBS) solution to ensure spermatozoa remobilization and three independent sperm count ( $\times 10^6$ ,  $n=3$ ) were assessed using a Malassez slide (20-fold and 100-fold dilution for tail and head of epididymis respectively).

### 2.3.3. Immunohistochemistry

Testicular immunohistological analyses were conducted according to the manufacturer's recommendations. Briefly, 5 µm sections were mounted on positively charged glass slides (Superfrost plus) before being deparaffinized, rehydrated, treated for 20 min at 93–98 °C in 0.01 M citric buffer–Tween 0.1% (pH 6), rinsed in osmosed water (2 x 5 min), and washed (2 x 5 min) in phosphate-buffered saline (PBS). Thin sections were then incubated in blocking solutions (PBS 1x + 10% FBS-fetal bovine serum) for 1h at room temperature. Primary SOX9 (Millipore, AB5535), SYCP3 (Abcam, 97672), PLZF (Santa Cruz, SC-28319) and acetyl-Histone H4 (H4ac, Millipore, 06-946) antibodies were then diluted in blocking solution and applied to samples overnight at 4°C. After several washes in PBS 1x, a first step of polymeric amplification with HRP (horse-radish polymerase) were performed for 30 min at room temperature (only for SYCP3 and PLZF antibodies). Fluorophore-conjugated secondary antibodies were then applied for 1h at room temperature. After several washes in PBS 1x, the slides were then counterstained with Hoechst medium (1 mg/mL) (Invitrogen, Cergy Pontoise, France), mounted on PBS/glycerol (50 % v/v) and imaged with a Zeiss Axioscan Microscope Slide Scanner. Immunohistochemical quantification were then performed on the open source QuPath software to count the proportion of normal seminiferous tubules. This proportion was estimated by counting (i) the number of PLZF and SOX9 positive cells per seminiferous tubules and (ii) the number of seminiferous tubules with H4ac. and SYCP3 positive cells normalized to the total number of tubules. For each section, all the rounded seminiferous tubules were counted ( $n > 20$ ). All the data are reported in Supp. Table 6.

## 2.4. Major and trace elements

All chemical analyses were carried out in clean laminar flow hoods using double-distilled acids to avoid any exogenous contaminations.

All the biological samples including freeze-dried organs, blood, urine and mice food, were dissolved in a concentrated  $\text{HNO}_3\text{-H}_2\text{O}_2$  mixture in Savillex beakers at  $100^\circ\text{C}$  for at least 72 h. After complete digestion, major and trace element concentrations were measured in a small aliquot on an ICP-AES (Agilent 5800) and a quadrupole ICP-MS (Agilent 7500), respectively, at the Laboratoire Magmas et Volcans (LMV) following the method described in Garçon et al.,<sup>34</sup>. When necessary, analytical drift was corrected using indium (In) addition as internal standard for trace elements. The validity and reproducibility of major and trace element concentrations are estimated to be around 5% (2sd) based on re-run analysis (bis) and complete duplicates of international (*i.e.*, bovine liver, 1577c) biological reference material (see Supp. Table 2). Major and trace element concentrations are all reported in  $\mu\text{g/g}$  (ppm) and  $\text{ng/g}$  (ppb) dry weight respectively in Supp. Table 2.

For geological samples, before any measurements, volcanic ash was further ground in an agate mortar to ensure homogeneity. Major and trace concentrations were then quantified and are all reported in Supp. Table 7. For major elements, samples were first melted with lithium metaborate. Metaborate fusion products were then dissolved with nitric acid and like for biological samples, concentrations were determined on an ICP-AES (Agilent 5800). Loss on ignition (LOI) was measured by weighing the bulk sample before and after 1 h of calcination at  $1000^\circ\text{C}$ . For trace elements, samples were directly dissolved in a concentrated  $\text{HF-HNO}_3$  (1:3) mixture at  $90^\circ\text{C}$  for at least 48 h before evaporation and resuspension in a concentrated  $\text{HNO}_3$  - 6N HCl (1:1) mixture at  $90^\circ\text{C}$  for 24 h. This step was repeated three times. Trace element concentrations were measured on a quadrupole ICP-MS (Agilent 7500). Both accuracy and reproducibility of the major and trace element contents were monitored by replication of international rock standards (BHVO<sub>2</sub>). The concentration obtained for the standards are in agreement with the reference values, and reproducibility is, on average, better than 5% for the trace and 10% (2sd) for the major elements (see Supp. Table 7).

Note that beyond the total digestion procedure used in this study to assess the entire metallomic signature of the geological samples, another parameter termed the bioaccessibility (performed with water, synthetic gastric and/or lung fluids) may help to refine metal exposure assessment<sup>37-39</sup>. In this preliminary study, in the absence of established analytical protocols and the lack of significant databases, in particular with regard to isotopic data, we however undertook to first maximize the risk resulting from metallome deregulations induced by long-term volcanic ash exposure via a total dissolution procedure. In future studies, measuring the chemical and for the first time the copper and zinc isotopic bioaccessibility might however be useful to better constrain this volcanic hazard.

## 2.5. Cu and Zn isotopic compositions

Copper (Cu) and zinc (Zn) isotopic compositions were measured following the procedure described by Maréchal et al.<sup>40</sup>. Cu and Zn were purified using quartz columns filled with 1.8 mL of Bio-Rad AG MP-1 (100-200 mesh) anion exchange resin. After removing the matrix phase with 10 mL of 7N HCl + 0.001%  $\text{H}_2\text{O}_2$ , Cu was first eluted with 20 mL of the same solution, followed by Zn with 10 mL of a 0.5N  $\text{HNO}_3$  solution. Total procedural blanks were less than 6 ng for Zn and lower than 2 ng for Cu which is well below the amount of these elements in all the samples (on average Zn and Cu > 200 ng except for urine in which Zn and Cu ~ 50 ng).

Isotopic compositions were measured on a Thermo Scientific Neptune Plus MC-ICP-MS using standard sample and skimmer cones in wet plasma conditions (*i.e.*, no desolvating nebulizer system (DSN) with cycloning introduction chamber and a  $50\mu\text{L/min}$  glass nebulizer). On the day of the analyses, Zn and Cu purified solutions were diluted in a Cu (Cu SRM 976, National Institute of Standards and Technology, Gaithersburg, MD, USA) and Zn-doped solution (Zn JMC 3-0749L, Johnson Matthey Royston, UK) respectively, to match the concentration of the standard mixture ran between the samples (about  $250\mu\text{g.L}^{-1}$ ). The delta

values (expressed in ‰) are reported relative to the isotopic solution reference material NIST SRM 976 for Cu and JMC 3-0749L for Zn and are referred as:

$$\delta^{65}\text{Cu}_{\text{sample}} = \left[ \frac{\left( \frac{^{65}\text{Cu}}{^{63}\text{Cu}} \right)_{\text{sample}}}{\left( \frac{^{65}\text{Cu}}{^{63}\text{Cu}} \right)_{\text{SRM976}}} - 1 \right] * 10^3 \text{ and } \delta^{66}\text{Zn}_{\text{sample}} = \left[ \frac{\left( \frac{^{66}\text{Zn}}{^{64}\text{Zn}} \right)_{\text{sample}}}{\left( \frac{^{66}\text{Zn}}{^{64}\text{Zn}} \right)_{\text{JMC3-0749L}}} - 1 \right] * 10^3$$

Instrumental mass fractionation was corrected with an exponential law using an elemental-doping method and instrumental drift over time was controlled with standard sample bracketing<sup>40</sup>.

The long-term precision of the results was assessed by sample re-run analysis (bis) and repeated measurements of the pure Cu SRM 976 and Zn JMC 3-0749L standard solutions run every two samples and the accuracy was assessed by the measurement of biological (1577c) and geological (BHVO<sub>2</sub>) international reference materials. The reproducibility (2sd) of the Cu SRM 976 and Zn JMC 3-0749L standards was better than 0.07‰ (n=150) for both  $\delta^{65}\text{Cu}$  and  $\delta^{66}\text{Zn}$ . Our results for the reference standards are 0.08 ‰ (2sd, n=8) for 1577c and 0.04 ‰ (2sd, n=5) for BHVO<sub>2</sub> for  $\delta^{65}\text{Cu}$  ( $\delta^{65}\text{Cu}_{1577\text{c}} = +0.27 \pm 0.08$  (2sd, n = 8),  $\delta^{65}\text{Cu}_{\text{BHVO}_2} = +0.06 \pm 0.04$  (2sd, n = 5)) and are 0.04 ‰ (2sd, n=8) for 1577c and 0.01 ‰ (2sd, n=5) for BHVO<sub>2</sub> for  $\delta^{66}\text{Zn}$  ( $\delta^{66}\text{Zn}_{1577\text{c}} = -0.21 \pm 0.04$  (2sd, n = 8),  $\delta^{66}\text{Zn}_{\text{BHVO}_2} = +0.32 \pm 0.01$  (2sd, n = 5) (cf Supp. Tables 2 and 7). All these values are in good agreement with certified and previous published values *i.e.*,  $\delta^{65}\text{Cu}_{1577\text{c-ref}} = +0.37 \pm 0.05$  (2sd) and  $\delta^{66}\text{Zn}_{1577\text{c-ref}} = -0.19 \pm 0.05$  (2sd)<sup>41</sup> and  $\delta^{65}\text{Cu}_{\text{BHVO}_2\text{-ref}} = +0.09 \pm 0.06$  (2sd) and  $\delta^{66}\text{Zn}_{\text{BHVO}_2\text{-ref}} = +0.27 \pm 0.05$  (2sd) (source: Georem). Given our long-term precision and the accuracy obtained on reference material measurements, the two-standard deviation (2sd) analytical uncertainty adopted in this study for the Cu and Zn isotopic compositions is  $\pm 0.07$  ‰.

### 3. Results

#### 3.1. Geological samples

The lab-crushed volcanic ash has a median grain size of ~100 µm (3.5Φ) (Supp. Figure 1b). It has a dacitic composition with a high SiO<sub>2</sub> (69.25 ± 0.60 % (2sd), n = 5) and a low Na<sub>2</sub>O+K<sub>2</sub>O (1.83 ± 0.22 % (2sd), n = 5) content (Supp. Figure 1c). More generally, it has relatively high major element contents (Ti, Al, Fe, Mn, Mg, Ca, Na and K) compared to a wide spectrum of worldwide volcanic ash, although these values remain lower or equivalent to those measured in the upper continental crust (UCC) (Supp. Figure 3). Inversely, for trace elements and more particularly metals, it has relatively high values compared to previously reported data for several worldwide volcanic ash which can exceed the average UCC values (enrichment factor > 1) as shown for example for vanadium (V), copper (Cu), molybdenum (Mo) and cadmium (Cd) (Supp. Figure 3). Regarding the stable isotopic compositions, La Soufrière volcanic ash has a copper and zinc isotopic composition of -0.52 ± 0.11 ‰ (2sd, n = 5) and +0.18 ± 0.02 ‰ (2sd, n = 5) respectively (cf Supp. Table 7).

#### 3.2. Trace element concentrations and Cu-Zn isotopic compositions in biological samples

To evaluate the effect of chronic exposure to metal-rich volcanic ash on the entire body metallome, we used significant p-value boxplots (Supp. Figure 4) and principal component analyses (PCA) (Figure 2). Briefly, PCA is a mathematical algorithm that reduces the dimensionality of an original multivariate dataset by identifying new variables (principal components; PCs), defined as linear combinations of the original variables<sup>42</sup>. Such multivariate analysis method allows to preserve and visualize the main relevant information in a new PC1 vs PC2 space. Our results show that, independently of ash exposure, the mice metallome is organ-specific (Figure 2 and Supp. Figure 5) and isotopically-typified (Figure 3) as previously described in the literature<sup>43,44</sup>. After one month of ash exposure, the latter tend to be highly disrupted as shown for example by the significant (p-value < 0.05) heavy and alkaline metal accumulation (Zn, Fe, Mn, Ca, Mg, K, P) (Supp. Figure 4) associated to an upward trend for copper (Figure 4a), cobalt and vanadium (0.05 < p-value < 0.1) in the testes. Similarly, after one month of exposure, the blood reservoir is significantly enriched (p-value < 0.05) in

vanadium (V), iron (Fe) selenium (Se) and cerium (Ce) (Supp. Figure 4). When still focusing on the elemental concentrations, the intestine, the brain, the lung, the heart and the kidney are also subjected to metallome deregulations but to a lesser extent. For example, the only major variation observed in the lung is limited to V increase while for the intestine the V, Fe and Co enrichments are counterbalanced by strontium (Sr), manganese (Mn), Cu, arsenic (As) and calcium (Ca) decrease (Supp. Figure 4). Another noticeable feature, so far never observed, is the significant ~0.3 ‰ copper isotopic decrease observed in liver and intestine in association to a Cu drop after one month of exposure (Figure 3a and Supp. Figure 4) associated with small but not significant zinc isotopic variations in blood, urine and kidney (Figure 3b). All these results, besides complementing previous studies, show for the first time that, in addition to external body parts like urine, scalp hair<sup>18</sup> or mice tail<sup>45</sup>, internal organs are also significantly affected by metallome disruption. Note that all these elemental deregulations are organ and fluid-dependent, with testes, blood, urine and to a lesser extent liver presenting a more pronounced disrupted metallome as illustrated by significant differences between the control and the exposed subjects (Figure 2a and Supp. Figure 4) than lung, brain, kidney, heart and intestine characterized by a more stable metallome over time exposure (Figure 2b and Supp. Figure 4).

### 3.3. Ash-related pathophysiological deregulations

In association with internal metallome deregulations, we observed external and morphological features after one month of exposure. The most obvious is a decrease of food (Supp. Figure 2a) and water (Supp. Figure 2b) consumption although this has no direct impact on the body weight (Supp. Figure 2c). From a physiological point of view, our results demonstrate that the organs mostly affected by metallome deregulation (*i.e.*, testes, liver) are also marked by more pronounced physiological disturbances while all the other organs like kidney and lung maintain a stable structure over time exposure with no signs of evident intra-tissue damages (histological data not shown here). For testes, the main changes translate into a minimum 25 % decrease of spermatozoa in the head and in the tail of the epididymis *i.e.*, inadequate number of male germ cells (Figure 4b) associated with a significant number of visible microscopic lesions in the male reproductive system as highlighted by lower testicular epithelium thickness ( $p_{\text{Mann-Whitney U-test}} = 0.002$ ; Figure 4c), epithelial desquamation (Figure 5b,c), intratubular atypical germ cells (Figure 5d) and preliminary signs of interstitial fibrosis (Figure 5c), all accounting for significant tubular degeneration. Our results also demonstrates that volcanic ash exposure led to a significant decrease of the number of spermatids ( $p=0.039$ ) associated to a downward trend to lower Sertoli cells number ( $p=0.1797$ ), as revealed by acetyl-Histone H4 (H4ac.) and SOX9 immunostaining (Figure 6a). Inversely, the number of spermatogonia and spermatocytes seems to be preserved as shown by the similar number ( $p>0.2$ ) of seminiferous tubules marked by positive PLZF and SYCP3-stained cells in the control and the exposed group (Figure 6a). Altogether, these results suggest that chronic volcanic ash exposure seems to preferentially affect the last stages of spermatogenesis *i.e.*, spermatidogenesis and spermiogenesis without altering stem cells and spermatocytogenesis. Note that like for the decrease of the testicular epithelium thickness (Figure 4c), the most significant spermatids loss is observed in the exposed mice characterized by elevated amount of testicular heavy metals like Fe and Cu (Figure 6b and 6c).

For liver, although the histological sections do not show distinctive signs between the control and the exposed mice (not shown here), a significant decrease of the hepatic mass ( $p_{\text{Mann-Whitney U-test}}=0.002$ ) was noticed in the exposed mice in association with the copper isotopic decrease (Figure 7a).

## 4. Discussion

### 4.1. Volcanic-ash: a metal-rich reservoir that contributes to organ-specific metallome deregulations

In volcanic areas, the consumption of food<sup>16,46</sup> and water<sup>15,47</sup> contaminated by volcanogenic elements have been demonstrated to significantly biocontaminate the residents, as



documented by higher trace element contents in urine<sup>15</sup> and scalp hair<sup>18</sup> of people living in the vicinity of an active volcano compared to people of control areas. Over time, such volcanic-derived metallome disturbances might contribute to significant health risk and favor the development of severe diseases like thyroid cancer<sup>15,48</sup>, although, to our knowledge, no metallomic data has yet been reported for thyroid glands and more generally for vital organs to support this assumption. As the food chain is an important route of metal human exposure, other and more direct contamination induced for example by long-term exposure and subsequent ingestion of volcanic ash could also contribute to severe metal contamination. As they make up the majority of volcanic soils<sup>49</sup>, volcanic ash can be easily remobilized and absorbed by the organism, either by oral or dermal routes (up to 1000 mg per day<sup>50</sup> by oral ingestion) or by inhalation. La Soufrière volcanic ash is enriched in several chemical elements and particularly heavy metals such as Cu, Mo, V, Co, Cd, Fe and Mn, with values exceeding the ones reported for the upper continental crust (UCC) and well above the average content reported in several worldwide volcanic ash (Supp. Figure 3). Then, La Soufrière volcanic ash appears as an important metal reservoir to which direct and/or indirect (via food and water transfer) prolonged exposure may significantly deregulate the inner metallome. Our results demonstrate that, independently of ash exposure, the mice metallome is organ-specific (Supp. Figure 5) and isotopically-typed (Figure 3) as previously described<sup>43,51,52</sup>. However, after one month of exposure to metal-rich volcanic ash, the latter turn out to be highly disrupted, translating into both major and trace elements (Figure 2 and Supp. Figure 4) as well as  $\delta^{65}\text{Cu}$  and  $\delta^{66}\text{Zn}$  changes (Figure 3). Observed for the first time in inner organs, these variations are not systematic but rather organ-specific, with the liver and testes, in tandem with blood and urine (Figure 2a and Supp. Figure 4), being preferentially affected; as illustrated by more pronounced ash exposure-related metallome variations; compared to the brain, lung, heart, kidneys and intestine presenting a relatively more stable (e.g. lung) and/or counterbalanced (e.g. intestine) metallome over time exposure (Figure 2b and Supp. Figure 4). The most important variations are noted in testes (Figure 2a and Supp. Figure 4), the latter being characterized by a significant enrichment ( $p_{\text{wilcoxon-test}} < 0.05$ ) in Zn, Fe, Mn, Ca, K, Mg and P (Supp. Figure 4) and an upward trend for Cu, Co and V (e.g. Figure 4a) coupled with no Cu-Zn isotopic drift (Figure 3). Note that a similar enrichment tendency is also found in the blood reservoir as shown for example by higher V ( $p_{\text{wilcoxon-test}}=0.002$ ) and Fe ( $p_{\text{wilcoxon-test}}=0.026$ ) content in the exposed mice. The testicular heavy metal accumulation may result from the progressive disruption of the hemato-testicular barrier. As shown on Figure 6a, mice exposed to volcanic ash are characterized by a downward trend to lower Sertoli cells number in seminiferous tubules compared to the control mice, as demonstrated by the lower number of seminiferous tubules marked by positive SOX9-stained cells in the exposed group ( $\text{SOX9}^{+}_{\text{cells}}=9.63\pm 3.67$  (1sd)) versus the control group ( $\text{SOX9}^{+}_{\text{cells}}=12.16\pm 2.87$  (1sd)). Sertoli cells are somatic cells that form the blood-testis barrier and any decline, will directly translate into a progressive rupture of this barrier, favoring the transfer of heavy metals from the blood to the testis. The liver is inversely marked by a significant drop in  $\delta^{65}\text{Cu}$  (Figure 7) but a less pronounced major and trace content changes limited to the drop of copper (Supp. Figure 4), appearing as a more distinct case. Compared to the testes, the liver is a central organ in metal homeostasis that ensures a set of metabolic functions essential for the organism. By accounting for a large fraction of body metals such as copper, the liver stores, redistributes and excretes metal excess through urine, feces and bile<sup>53</sup>. The limited hepatic variations denoted for elemental concentrations is thus likely counterbalanced by preferential testicular and to a lesser extent blood metal accumulation and might result from an amplified protective mechanism resulting in higher metal urinary excretion, as supported by elevated chemical contents measured in the urine of exposed mice (see Figure 2a and Supp. Table 2). Altogether, these results suggest that liver functions, despite the presence of copper isotopic disruptions, tend to be maintained after one month of exposure to volcanic ash. Taken as a whole, all these results demonstrate that metal-rich volcanic ash acts as an external perturbation that rapidly disrupts the inner metal homeostasis at the entire body scale.

#### 4.2. Ash-related metallome deregulation and early pathophysiological modifications: the case of the testes

Metals like copper (Cu), zinc (Zn) and iron (Fe) are involved in several enzymes and proteins that regulate a set of metabolic pathways essential for the body functions including but not limited to cell energy (ATP) production, reactive oxygen species (ROS) detoxification<sup>53,54</sup>, spermatogenesis<sup>55</sup> and immune functions<sup>56</sup>. Metals are thus vital in the organism, but any homeostatic disturbance (accumulation, deficit, mislocalization as well as isotopic variation), as induced by chronic volcanic ash exposure (*cf* section 4.1), can play a reverse role in these processes and subsequently represent a significant health risk. Cu metallome deregulation is for example associated to neurodegenerative diseases<sup>23,57</sup> and cancer<sup>58</sup> development. Despite the well-established toxic effect of some metals and the recent observation that mammals (human and animal) living in a volcanic area are more prone to develop testicular damages<sup>45</sup>, multiple sclerosis<sup>14</sup> and cancers<sup>15,16</sup>, whether volcanic ash-derived metallome deregulation contributes to pathological dysfunctions and incidence of diseases in the volcanic areas has to be better constrained.

As detailed above, testes are the first organs severely affected by volcanic ash-induced metallome deregulation (Figure 2a and Supp. Figure 4). This preferential and targeted metallic disruption is associated with significant tubular degeneration as highlighted by inadequate number of germ cells including spermatids (Figure 6a) and spermatozoa in the head and the tail of the epididymis (Figure 4b). After one month of metal-rich volcanic ash exposure, significant microscopic lesions are also observed in the male reproductive system as shown by lower epithelium thickness (Figure 4c) associated with preliminary signs of epithelial desquamation (Figure 5b, c), interstitial destructure and inflammation (fibrosis) (Figure 5c). Testes of mice exposed to volcanic ash present also a larger number of uncommitted and atypically-localized intratubular germ cells within the seminiferous tubules strongly resembling to the so-called atypical residual bodies (Figure 5d); as many symptoms, although present in small quantity, that remain absent in the control group (Figure 5a). Abnormal residual bodies (ARB) have been described as the result from impaired maturation of germ cells and/or altered Sertoli cell processing of these remnants, reflecting germ cell degeneration<sup>59</sup>. Although their origin is still unclear, they have been described in rats following administration of tri-o-cresyl phosphate<sup>60</sup> and of a by-product of water disinfection, dibromoacetic acid<sup>61</sup> appearing as a chemically treatment-related fingerprint. In this study, the higher incidence of ARB-like compounds coupled with lower spermatozoa and spermatids as well as a decreased epithelium thickness observed on mice presenting the most pronounced testicular metallome deregulation (Figures 4b, 4c and Figures 6b, 6c) may thus attest of a metal-rich ash exposure-mediated testicular toxicity preferentially resulting from altered spermatido- and spermiogenesis. This observation is further supported by previous studies demonstrating that excess of Cu and other heavy metals such as Pb and Cd, reduce sperm count, mobility, vitality and morphology and subsequently affect male reproductive capacity<sup>62,63</sup>. In excess, heavy metals can also favor the production of reactive oxygen species (ROS) via the Fenton reaction<sup>64</sup> that may also contribute to testicular defects and subsequent infertility<sup>65</sup>. Altogether, these results show that volcanic ash-derived metallome deregulations is far from trivial and may, to a certain extent, contribute during lifetime to severe fertility disorders.

#### 4.3. Copper and zinc isotopic compositions: a promising tool to diagnose hepatic ash-related dysfunctions?

Beyond elemental concentrations, another significant metallomic parameter disrupted by volcanic ash exposure and observed for the first time in this study is Cu isotopic decrease in both liver and intestine (Figure 3) and, in a less pronounced way, Zn isotopic fractionation in blood, urine and kidney respectively. Independent of the amount of metals, the Cu and Zn isotopic compositions ( $\delta^{65}\text{Cu}$ ,  $\delta^{66}\text{Zn}$ ) are promising tools that recently offer a more comprehensive view of several biological processes than concentrations alone such as aging<sup>20,21,66</sup>. They also turned out to be very promising tools for pointing out a disruption in the oxidative stress status<sup>67</sup>, a major pathogenetic event occurring in several liver disorders<sup>68</sup>, and more broadly for the diagnosis, prognosis and follow-up of patients suffering from severe

pathologies like cancers<sup>22,69</sup>, neurodegenerative diseases<sup>23,70,71</sup> as well as severe hepatic syndromes<sup>72–75</sup>; with the amplitude of the variations being likely linked to the severity of the disease<sup>73,75</sup>. Despite this proven interest, the use of  $\delta^{65}\text{Cu}$  and  $\delta^{66}\text{Zn}$  as a potential marker for health prevention have never been investigated in a volcanically active context. Here we demonstrate that mice exposed to volcanic ash present a significant hepatic  $\delta^{65}\text{Cu}$  drop, following a pattern similar to mice suffering from hepatic diseases<sup>72</sup> and associated with a hepatic mass loss up to 20% (Figure 7a). Organ weight, and more specifically liver mass loss, is an important parameter for the evaluation of toxicity. Described as a common background finding in elderly<sup>76</sup> and attributed to portal venous blood flow (PVBF) disturbance<sup>77</sup>, PVBF-related liver mass reduction is also an ubiquitous pattern observed in patients suffering from severe liver diseases such as hepatocellular carcinoma (HCC) and liver cirrhosis<sup>78</sup>. Hepatic mass loss was also noticed in rats' livers in response to increase oxidative stress caused by metal exposure<sup>79</sup>. In the absence of age variations and other markers commonly associated with advanced liver dysfunctions such as histological lesions, the hepatic mass loss in correlation with the  $\delta^{65}\text{Cu}$  decrease (Figure 7a) might be considered as the preliminary warning signs of an ongoing severe liver metabolic disruption. At this stage, the cause of these copper isotopic fractionations remains to be elucidated, but given previous studies, the latter may result from modified copper protein expression, including the superoxide dismutase (Cu-Zn SOD1) in association to enhanced oxidative conditions. These two parameters, identified as precursors in the development of hepatocellular carcinoma<sup>80</sup>, have been demonstrated to impact copper isotopic fractionation<sup>67,81</sup>.

More broadly, hepatic  $\delta^{65}\text{Cu}$  decrease may also reflect ongoing impairments that could be generalized at the entire enterohepatic cycle. As shown on Figure 3a and Supp. Figure 6, after one month of exposure, the hepatic  $\delta^{65}\text{Cu}$  decrease is associated with a significant intestinal  $\delta^{65}\text{Cu}$  drop. Although the most evident process to explain such Cu isotopic variability is the presence of volcanic particles having light Cu isotopic composition ( $\delta^{65}\text{Cu}_{\text{ash}} = -0.52 \pm 0.11\text{‰}$ ) in the liver and the intestinal tractus, none were observed in any of the histologically quantified organs including liver. Inversely, intestinal Cu uptake is largely mediated by two major membrane transporters (CTR1 and DMT1) and metalloredutase (STEAP proteins)<sup>53</sup> which alteration has been demonstrated to significantly affect  $\delta^{65}\text{Cu}$ <sup>82</sup>. The light intestinal  $\delta^{65}\text{Cu}$  observed in the exposed mice thus likely results from impaired Cu gut uptake, directly echoing to altered food consumption (Supp. Figure 2). Once absorbed, Cu is incorporated into the nutrient rich blood and transported through the portal vein from the gut to the liver. This subsequently impacts the  $\delta^{65}\text{Cu}$  liver as supported by the correlation observed between hepatic and intestinal  $\delta^{65}\text{Cu}$  (Supp. Figure 6).

Monitoring liver  $\delta^{65}\text{Cu}$  may thus offer new perspectives to alert on the early development of (entero)hepatic deregulations in volcanic areas. The measurement of hepatic  $\delta^{65}\text{Cu}$  will however require a biopsy *i.e.* an invasive surgical intervention that may limit the scope of this marker. But this might be overcome with less invasive blood tests. As highlighted on Figure 7b, the hepatic  $\delta^{65}\text{Cu}$  correlates with the blood  $\delta^{66}\text{Zn}$ , suggesting that the blood  $\delta^{66}\text{Zn}$  might be an equally robust but far less invasive biomarker. To date, although the simultaneous measurement of hepatic  $\delta^{65}\text{Cu}$  and blood  $\delta^{66}\text{Zn}$  remains mandatory to ensure that the blood isotopic variations really reflect hepatic disorders, in the future, this will allow to move towards less invasive techniques only focused on blood isotopic analyses. All these results, beyond being innovative, are highly promising for all countries with a large population living in proximity to the volcanoes such as Peru, marked by an atypical age-specific pattern of hepatocellular carcinomas (HCCs)<sup>83</sup>, and more generally for developing countries in which more than 80% of HCCs occur<sup>84</sup> and for which, no reliable diagnosis markers are currently available<sup>85</sup>.

## 5. Conclusions and Perspectives

Our study reveals that mice chronically exposed to volcanic ash deposits present an organ-specific and isotopically-typified metallome deregulation. These deregulations, observed for the first time at the whole-body scale, confirm that volcanic ash is a major metal-rich contaminant that can seriously influence exposure to and intake of trace elements. In addition

to urine and blood, testes and, to a lesser degree, liver turned out to be preferentially affected by these ash-related metallome disruptions, which, after a month, are associated with pronounced pathophysiological changes. In the testes, this translates into an alteration of the spermatogenesis, attesting of a metal-rich ash exposure-mediated testicular toxicity. Beyond chemical concentrations, copper and zinc stable isotopic compositions were, for the first time, quantified at the entire body scale. Our results demonstrate that the liver, the intestine and to a lesser extent the blood are affected by  $\delta^{65}\text{Cu}$  and  $\delta^{66}\text{Zn}$  variations, that may be interpreted as the warning signs of coming up (entero)hepatic diseases. The analysis of hepatic  $\delta^{65}\text{Cu}$  and blood  $\delta^{66}\text{Zn}$ , may thus appear as a promising and innovative technique to diagnose severe liver dysfunctions preponderant in some developing and volcanic countries. In perspective, bio- and isotopically-monitoring human fertility and more broadly (entero)hepatic disorders in populations living in volcanic areas would bring valuable insights to confirm the findings of this study.

## Acknowledgements

We gratefully acknowledge Jean-Marie Nedelec of the Chemistry Institute of Clermont-Ferrand (ICCF) for his help in the grainsize characterization of the geological ash samples as well as Chantal Bosq, Abdel-Mouhcine Gannoun, Jean-Luc Piro, Mhammed Benbakkar and Claire Fonquernie of the Laboratoire Magmas and Volcans (LMV) for their assistance in the clean laboratory as well as during isotopic, trace and major element measurements respectively. We are also grateful to Fanny Perrière (Laboratoire Microorganismes, Génome Environnement, LMGE) for her technical support to freeze-dry the biological samples. Thanks are also due to Sandrine Plantade, Khirredine Ouchen, Philippe Mazuel for their help at the animal facility as well as Laura Thirouard and Sabrina Dehay of the Institute of Genetics, Reproduction and Development (iGReD) for helping us in the histological data preparation and interpretation. We also thank the AniPath platform from the iGReD for histological analyses. This research was financed by the French government IDEX-ISITE initiative 16-IDEX-0001 (CAP 20-25). This is a Laboratory of Excellence ClerVolc contribution number 513.

## References

1. Takahashi, T. & Shoji, S. Distribution and Classification of Volcanic Ash Soils. *Global Environ. Res.* **6**, 16 (2001).
2. Small, C. & Naumann, T. The global distribution of human population and recent volcanism. *Environmental Hazards* **3**, 93–109 (2001).
3. Shoji, S., Dahlgren, R. & Nanzyo, M. Chapter 1 Terminology, Concepts and Geographic Distribution of Volcanic Ash Soils. in *Developments in Soil Science* vol. 21 1–5 (Elsevier, 1993).
4. Simkin, T. & Siebert, L. *Earth's volcanoes and eruptions: an overview*. Sigurdsson, H. (ed.), *Encyclopedia of Volcanoes*. San Diego: Academic, pp. 249–262. (2000).
5. Ayris, P. M. & Delmelle, P. The immediate environmental effects of tephra emission. *Bull Volcanol* **74**, 1905–1936 (2012).
6. Tomašek, I. *et al.* Assessing the biological reactivity of organic compounds on volcanic ash: implications for human health hazard. *Bull Volcanol* **83**, 30 (2021).
7. Green, F. H. Y. *et al.* Is volcanic ash a pneumoconiosis risk? *Nature* **293**, 216–217 (1981).
8. Lee, S. H. & Richards, R. J. Montserrat volcanic ash induces lymph node granuloma and delayed lung inflammation. *Toxicology* **195**, 155–165 (2004).
9. Sanders, C. L., Rhoads, K. & Mahaffey, J. A. Long-Term Reactivity of Lung and Mediastinal Lymph Nodes following Intratracheal Instillation of Sandy Loam Soil or Mount St. Helens Volcanic Ash'. *Environmental Research* **32**, 188–198 (1983).
10. Aguilera, C. *et al.* Biological Impact of Exposure to Extremely Fine-Grained Volcanic Ash. *Journal of Nanotechnology* **2018**, 1–12 (2018).
11. Damby, D. E. *et al.* Volcanic Ash Activates the NLRP3 Inflammasome in Murine and

- Human Macrophages. *Front. Immunol.* **8**, 2000 (2018).
12. Damby, D. E., Murphy, F. A., Horwell, C. J., Raftis, J. & Donaldson, K. The in vitro respiratory toxicity of cristobalite-bearing volcanic ash. *Environmental Research* **145**, 74–84 (2016).
13. Baxter, P. J., Ing, R., Falk, H. & Plikaytis, B. Mount St. Helens Eruptions: The Acute Respiratory Effects of Volcanic Ash in a North American Community. *Archives of Environmental Health: An International Journal* **38**, 138–143 (1983).
14. Nicoletti, A. *et al.* Incidence of multiple sclerosis in the province of Catania. A geo-epidemiological study. *Environmental Research* **182**, 109022 (2020).
15. Malandrino, P. *et al.* Increased thyroid cancer incidence in a basaltic volcanic area is associated with non-anthropogenic pollution and biocontamination. *Endocrine* **53**, 471–479 (2016).
16. Türkdoğan, M. K., Kilicel, F., Kara, K., Tuncer, I. & Uygan, I. Heavy metals in soil, vegetables and fruits in the endemic upper gastrointestinal cancer region of Turkey. *Environmental Toxicology and Pharmacology* **13**, 175–179 (2003).
17. Leung, C. C., Yu, I. T. S. & Chen, W. Silicosis. *The Lancet* **379**, 2008–2018 (2012).
18. Varrica, D., Tamburo, E., Dongarrà, G. & Sposito, F. Trace elements in scalp hair of children chronically exposed to volcanic activity (Mt. Etna, Italy). *Science of The Total Environment* **470**, 117–126 (2014).
19. Lobinski, R., Becker, J. S., Haraguchi, H. & Sarkar, B. Metallomics: Guidelines for terminology and critical evaluation of analytical chemistry approaches (IUPAC Technical Report). *Pure and Applied Chemistry* **82**, 493–504 (2010).
20. Sauzéat, L., Laurençon, A. & Balter, V. Metallome evolution in ageing *C. elegans* and a copper stable isotope perspective. *Metallomics* **10**, 496–503 (2018).
21. Morel, J.-D. *et al.* The mouse metallomic landscape of aging and metabolism. *Nature Communications* **10** (2022) doi:<https://doi.org/10.1038/s41467-022-28060-x>.
22. Balter, V. *et al.* Natural variations of copper and sulfur stable isotopes in blood of hepatocellular carcinoma patients. *PNAS* **112**, 982–985 (2015).
23. Sauzéat, L. *et al.* Isotopic Evidence for Disrupted Copper Metabolism in Amyotrophic Lateral Sclerosis. *iScience* **6**, 264–271 (2018).
24. Guern, F. L., Bernard, A. & Chevrier, R. M. Soufrière of Guadeloupe 1976-1977 Eruption - Mass and Energy Transfer and Volcanic Health Hazards (\*). *Bulletin of Volcanology* **43–3**, 577–593 (1980).
25. Moretti, R. *et al.* The 2018 unrest phase at La Soufrière of Guadeloupe (French West Indies) andesitic volcano: Scrutiny of a failed but prodromal phreatic eruption. *Journal of Volcanology and Geothermal Research* **393**, 106769 (2020).
26. Jessop, D. E. *et al.* A multi-decadal view of the heat and mass budget of a volcano in unrest: La Soufrière de Guadeloupe (French West Indies). *Bull Volcanol* **83**, 16 (2021).
27. Bilan mensuel de l'activité volcanique de la Soufrière de Guadeloupe et de la sismicité régionale. OVSG-IPGP Octobre 2021; ISSN 1622-4523. DOI: [http://volcano.ipgp.fr/guadeloupe/Bulletins/2021/OVSG\\_2021-10\\_fra.pdf](http://volcano.ipgp.fr/guadeloupe/Bulletins/2021/OVSG_2021-10_fra.pdf). (2021).
28. Sigurdsson, H., Houghton, B., McNutt, S., Rymer, H. & Stix, J. *The encyclopedia of Volcanoes*. (Elsevier Science (Eds.), 2015).
29. Komorowski, J.-C. *et al.* *Volcanic Hazard Atlas of the Lesser Antilles. Guadeloupe, in: Lindsay, J.M., Robertson, R.E.A., Shepherd, J.B., Ali, S. (Eds.), pp. 65-102.* (2005).
30. Martel, C., Pichavant, M., Balcone-Boissard, H. & Boudon, G. Syn-Eruptive Conditions of the AD 1530 Sub-Plinian Eruption of La Soufrière of Guadeloupe (Lesser Antilles). *Front. Earth Sci.* **9**, 686342 (2021).
31. Osman, S., Beckett, F., Rust, A. & Snee, E. Sensitivity of Volcanic Ash Dispersion Modelling to Input Grain Size Distribution Based on Hydromagmatic and Magmatic

- Deposits. *Atmosphere* **11**, 567 (2020).
32. Waterston, R.H., Lindblad-Toh, K. & Birney, E. Initial sequencing and comparative analysis of the mouse genome. *Nature* **420**, 520–562 (2002).
33. Rosenthal, N. & Brown, S. The mouse ascending: perspectives for human-disease models. *Nat Cell Biol* **9**, 993–999 (2007).
34. Garçon, M. *et al.* Nitrile, Latex, Neoprene and Vinyl Gloves: A Primary Source of Contamination for Trace Element and Zn Isotopic Analyses in Geological and Biological Samples. *Geostandards and Geoanalytical Research* **41**, 367–380 (2017).
35. Keyzer, J. J. *et al.* Zinc in plasma and serum: influence of contamination due to the collection tubes. *Pharmaceutisch Weekblad Scientific Edition* **5**, 248–251 (1983).
36. Williams, D. M. Trace metal determinations in blood obtained in evacuated collection tubes. *Clinica Chimica Acta* **99**, 23–29 (1979).
37. Goix, S. *et al.* Metal concentration and bioaccessibility in different particle sizes of dust and aerosols to refine metal exposure assessment. *Journal of Hazardous Materials* **317**, 552–562 (2016).
38. Tomašek, I. *et al.* Development of a simulated lung fluid leaching method to assess the release of potentially toxic elements from volcanic ash. *Chemosphere* **278**, 130303 (2021).
39. Tomašek, I., Mileusnić, M. & Leboš Pavunc, A. Health impact assessment by ingestion of polluted soil/sediment. *MGPB* **31**, 29–39 (2016).
40. Maréchal, C. N., Télouk, P. & Albarède, F. Precise analysis of copper and zinc isotopic compositions by plasma-source mass spectrometry. *Chemical Geology* **156**, 251–273 (1999).
41. Sauzéat, L. *et al.* Inter-comparison of stable iron, copper and zinc isotopic compositions in six reference materials of biological origin. *Talanta* **221**, 121576 (2021).
42. Ringnér, M. What is principal component analysis? *Nat Biotechnol* **26**, 303–304 (2008).
43. Balter, V. *et al.* Contrasting Cu, Fe, and Zn isotopic patterns in organs and body fluids of mice and sheep, with emphasis on cellular fractionation. *Metallomics* **5**, 1470 (2013).
44. Moynier, F., Fujii, T., Shaw, A. S. & Le Borgne, M. Heterogeneous distribution of natural zinc isotopes in mice. *Metallomics* **5**, 693 (2013).
45. Ferreira, A. F., Garcia, P. V., Camarinho, R. & Rodrigues, A. dos S. Volcanogenic pollution and testicular damage in wild mice. *Chemosphere* **132**, 135–141 (2015).
46. Orellana, E. *et al.* Heavy Metals in Native Potato and Health Risk Assessment in Highland Andean Zones of Junín, Peru. *JEP* **11**, 921–937 (2020).
47. Loma, J. D. Arsenic Exposure and Cancer-Related Proteins in Urine of Indigenous Bolivian Women. *Frontiers in Public Health* **8**, 11 (2020).
48. Vigneri, R., Malandrino, P., Gianì, F., Russo, M. & Vigneri, P. Heavy metals in the volcanic environment and thyroid cancer. *Molecular and Cellular Endocrinology* **457**, 73–80 (2017).
49. Delmelle, P., Opfergelt, S., Cornelis, J.-T. & Ping, C.-L. The Encyclopedia of Volcanoes (Second Edition). *Part IX: Economic Benefits and Cultural Aspects of Volcanism* 1253–1264 (2015) doi:10.1016/b978-0-12-385938-9.00072-9.
50. Moya, J. & Phillips, L. A review of soil and dust ingestion studies for children. *Journal of Exposure Science & Environmental Epidemiology* **24**, 545–554 (2014).
51. Ma, S. *et al.* Organization of the Mammalian Ionome According to Organ Origin, Lineage Specialization, and Longevity. *Cell Reports* **13**, 1319–1326 (2015).
52. Zhang, B., Podolskiy, D. I., Mariotti, M., Seravalli, J. & Gladyshev, V. N. Systematic age-, organ-, and diet-associated ionome remodeling and the development of ionomic aging clocks. *Aging Cell* **19**, (2020).
53. Kim, B.-E., Nevitt, T. & Thiele, D. J. Mechanisms for copper acquisition, distribution

and regulation. *Nature Chemical Biology* **4**, 176–185 (2008).

54. Turski, M. L. & Thiele, D. J. New Roles for Copper Metabolism in Cell Proliferation, Signaling, and Disease\*. *Journal of Biological Chemistry* **284**, 717–721 (2009).

55. Vallee, B. L. & Falchuk, K. H. The biochemical basis of zinc physiology. *Physiological Reviews* **73**, 79–118 (1993).

56. Bonaventura, P., Benedetti, G., Albarède, F. & Miossec, P. Zinc and its role in immunity and inflammation. *Autoimmunity Reviews* **14**, 277–285 (2015).

57. Barnham, K. J. & Bush, A. I. Metals in Alzheimer’s and Parkinson’s Diseases. *Current Opinion in Chemical Biology* **12**, 222–228 (2008).

58. Brady, D. C. *et al.* Copper is required for oncogenic BRAF signalling and tumorigenesis. *Nature* **509**, 492–496 (2014).

59. Creasy, D. *et al.* Proliferative and Nonproliferative Lesions of the Rat and Mouse Male Reproductive System. *Toxicol Pathol* **40**, 40S–121S (2012).

60. Somkuti, S. Light and electron microscopic evidence of tri-o-cresyl phosphate (TOCP)-mediated testicular toxicity in Fischer 344 rats. *Toxicology and Applied Pharmacology* **107**, 35–46 (1991).

61. Linder, R. E. *et al.* Histopathologic changes in the testes of rats exposed to dibromoacetic acid. *Reproductive Toxicology* **11**, 47–56 (1997).

62. Eidi, M. Seminal plasma levels of copper and its relationship with seminal parameters. *Iranian Journal of Reproductive Medicine* **8**, 60–65 (2010).

63. Roblero, L., Guadarrama, A., Lopez, T. & Zegers-Hochschild, F. Effect of copper ion on the motility, viability, acrosome reaction and fertilizing capacity of human spermatozoa in vitro. *Reprod. Fertil. Dev.* **8**, 871 (1996).

64. Betteridge, D. J. What Is Oxidative Stress? *Metabolism* **49**, Issue 2, Supplement 1, 3–8 (2000).

65. Asadi, N. The Impact of Oxidative Stress on Testicular Function and the Role of Antioxidants in Improving it: A Review. *JCDR* (2017) doi:10.7860/JCDR/2017/23927.9886.

66. Jaouen, K. *et al.* Is aging recorded in blood Cu and Zn isotope compositions? *Metallomics* **5**, 1016–1024 (2013).

67. Flórez, M. R., Costas-Rodríguez, M., Grootaert, C., Van Camp, J. & Vanhaecke, F. Cu isotope fractionation response to oxidative stress in a hepatic cell line studied using multi-collector ICP-mass spectrometry. *Anal Bioanal Chem* **410**, 2385–2394 (2018).

68. Ismail, N. *et al.* Antioxidant enzyme activities in hepatic tissue from children with chronic cholestatic liver disease. *Saudi J Gastroenterol* **16**, 90 (2010).

69. Larner, F. *et al.* Zinc isotopic compositions of breast cancer tissue. *Metallomics* **7**, 112–117 (2015).

70. Büchl, A., Hawkesworth, C. J., Ragnarsdottir, K. V. & Brown, D. R. Re-partitioning of Cu and Zn isotopes by modified protein expression. *Geochem Trans* **9**, 11 (2008).

71. Moynier, F., Foriel, J., Shaw, A. S. & Le Borgne, M. Distribution of Zn isotopes during Alzheimer’s disease. *Geochem. Persp. Let.* 142–150 (2017) doi:10.7185/geochemlet.1717.

72. Costas-Rodríguez, M. *et al.* Body distribution of stable copper isotopes during the progression of cholestatic liver disease induced by common bile duct ligation in mice. *Metallomics* **11**, 1093–1103 (2019).

73. Costas-Rodríguez, M. *et al.* Isotopic analysis of Cu in blood serum by multi-collector ICP-mass spectrometry: a new approach for the diagnosis and prognosis of liver cirrhosis? *Metallomics* **7**, 491–498 (2015).

74. Lamboux, A. *et al.* The blood copper isotopic composition is a prognostic indicator of the hepatic injury in Wilson disease. *Metallomics* **12**, 1781–1790 (2020).

75. Lauwens, S., Costas-Rodríguez, M., Van Vlierberghe, H. & Vanhaecke, F. Cu isotopic



- signature in blood serum of liver transplant patients: a follow-up study. *Sci Rep* **6**, 30683 (2016).
76. Kim, I. H., Kisseleva, T. & Brenner, D. A. Aging and liver disease: *Current Opinion in Gastroenterology* **31**, 184–191 (2015).
77. Zoli, M. Total and functional hepatic blood flow decrease in parallel with ageing. *Age and Ageing* **28**, 29–33 (1999).
78. Saftoiu, A., Ciurea, T. & Gorunescu, F. Hepatic arterial blood flow in large hepatocellular carcinoma with or without portal vein thrombosis: assessment by transcutaneous duplex Doppler sonography. *European Journal of Gastroenterology & Hepatology* **14**, 167–176 (2002).
79. Ogunrinola, O. O. *et al.* Effect of Low Level Cadmium Exposure on Superoxide Dismutase Activity in Rat. *Trop. J. Pharm Res* **15**, 115 (2016).
80. Wang, Z., Li, Z., Ye, Y., Xie, L. & Li, W. Oxidative Stress and Liver Cancer: Etiology and Therapeutic Targets. *Oxidative Medicine and Cellular Longevity* **2016**, 1–10 (2016).
81. Albarède, F. Metal Stable Isotopes in the Human Body: A Tribute of Geochemistry to Medicine. *ELEMENTS* **11**, 265–269 (2015).
82. Cadiou, J.-L. *et al.* Copper transporters are responsible for copper isotopic fractionation in eukaryotic cells. *Sci Rep* **7**, 44533 (2017).
83. Bertani, S. *et al.* An Atypical Age-Specific Pattern of Hepatocellular Carcinoma in Peru: A Threat for Andean Populations. *PLoS ONE* **8**, e67756 (2013).
84. Yang, J. D. & Roberts, L. R. Hepatocellular carcinoma: a global view. *Nat Rev Gastroenterol Hepatol* **7**, 448–458 (2010).
85. Asrani, S. K., Devarbhavi, H., Eaton, J. & Kamath, P. S. Burden of liver diseases in the world. *Journal of Hepatology* **70**, 151–171 (2019).

800  
801  
802  
803

**Figures:**

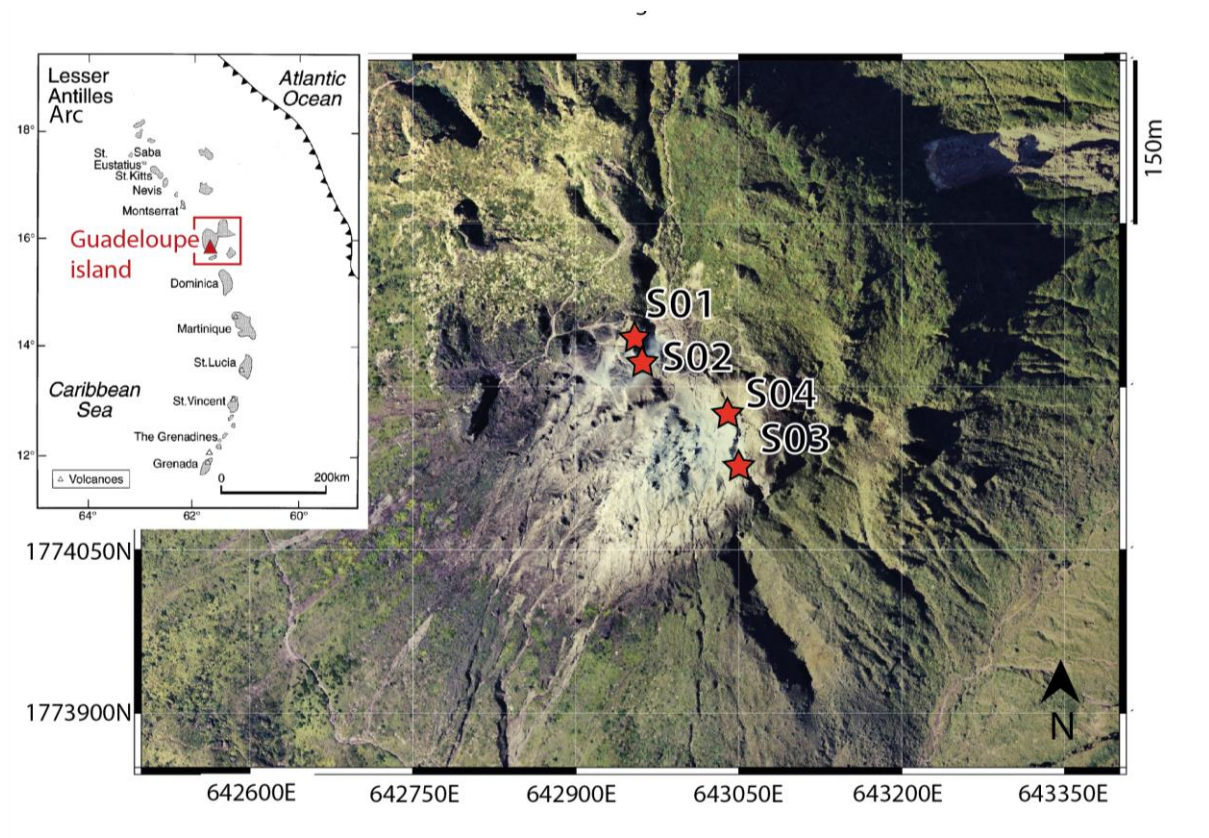


**Figure 1: Location map of the studied area**

Map of the Soufrière volcano located in the Guadeloupe island (Basse-Terre) of the Lesser Antilles arc (UTM coordinates). The red triangle indicate the location of the Soufrière volcano and the red stars indicate the sampling locations of the rocks from the volcanic dome (S01 to S04) used to reproduce «artificial» volcanic ash later exposed to mice in this study. S01 and S02 were collected on the «Tarissan» site while S03 and S04 are from the «Cratère Sud» site.

804

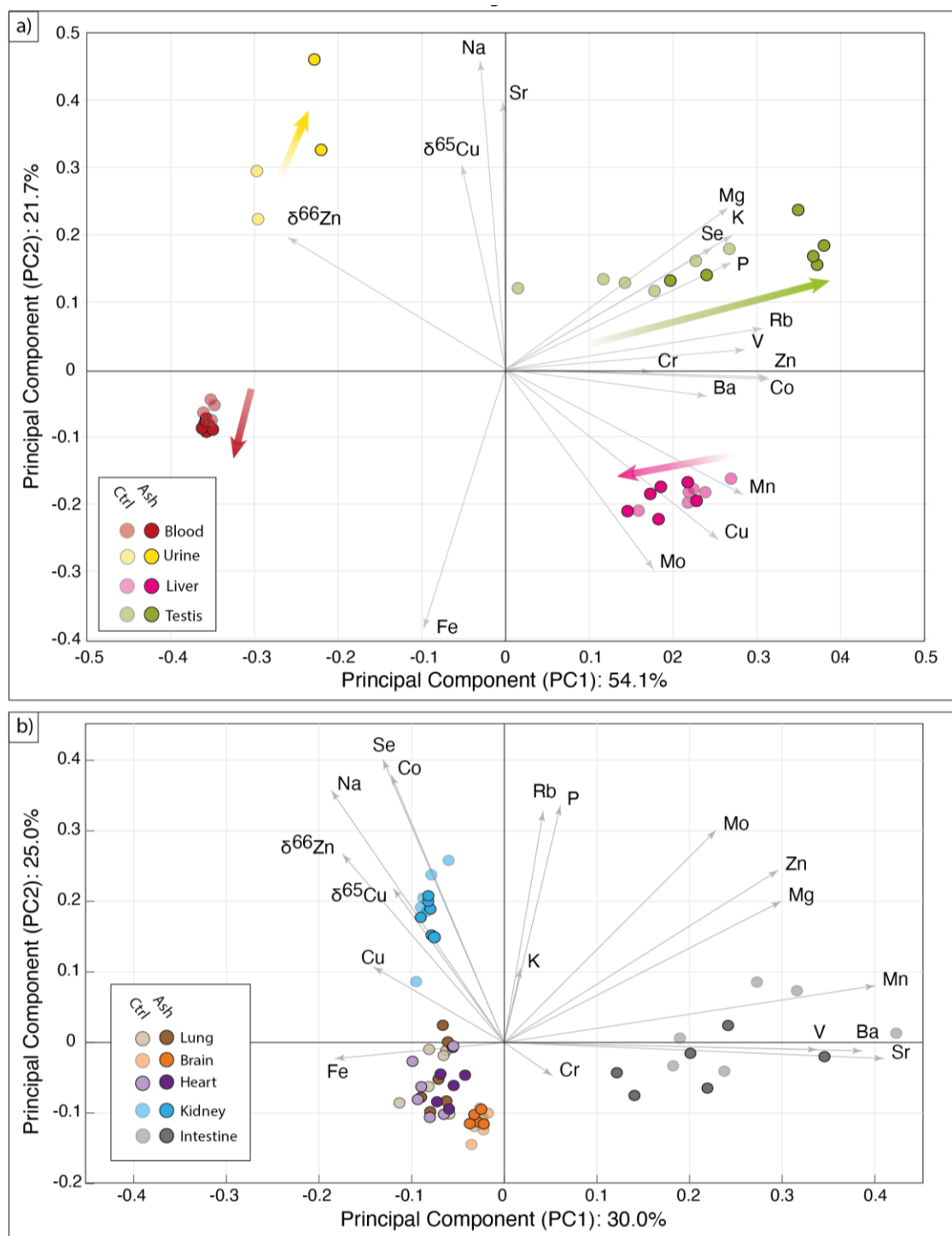


**Figure 2. Principal Component Analysis (PCA) of the Results**

The PCA allows (a) the identification of organs (i.e. testis and liver) and body fluids (i.e. blood and urine) preferentially affected by metallome deregulation (i.e. metallome difference between control and exposed subjects) due to volcanic ash exposure from (b) those that are less (i.e. no metallome difference between control and exposed subjects). In this study, the variables include the chemical concentrations of 16 major and trace elements measured in 7 organs and 2 biological fluids of mice, as well as  $\delta^{65}\text{Cu}$  and  $\delta^{66}\text{Zn}$  values. Grey arrows are graphic representations of loading factors in the new PC1 vs. PC2 space. The coordinates of each sample in the new PC1 vs PC2 space (i.e. sample scores) are shown by circles. Transparency and solid points stand for control and exposed subjects, respectively. All data were normalized, and samples with incomplete data were excluded. PCA was implemented in MATLAB<sup>TM</sup>.

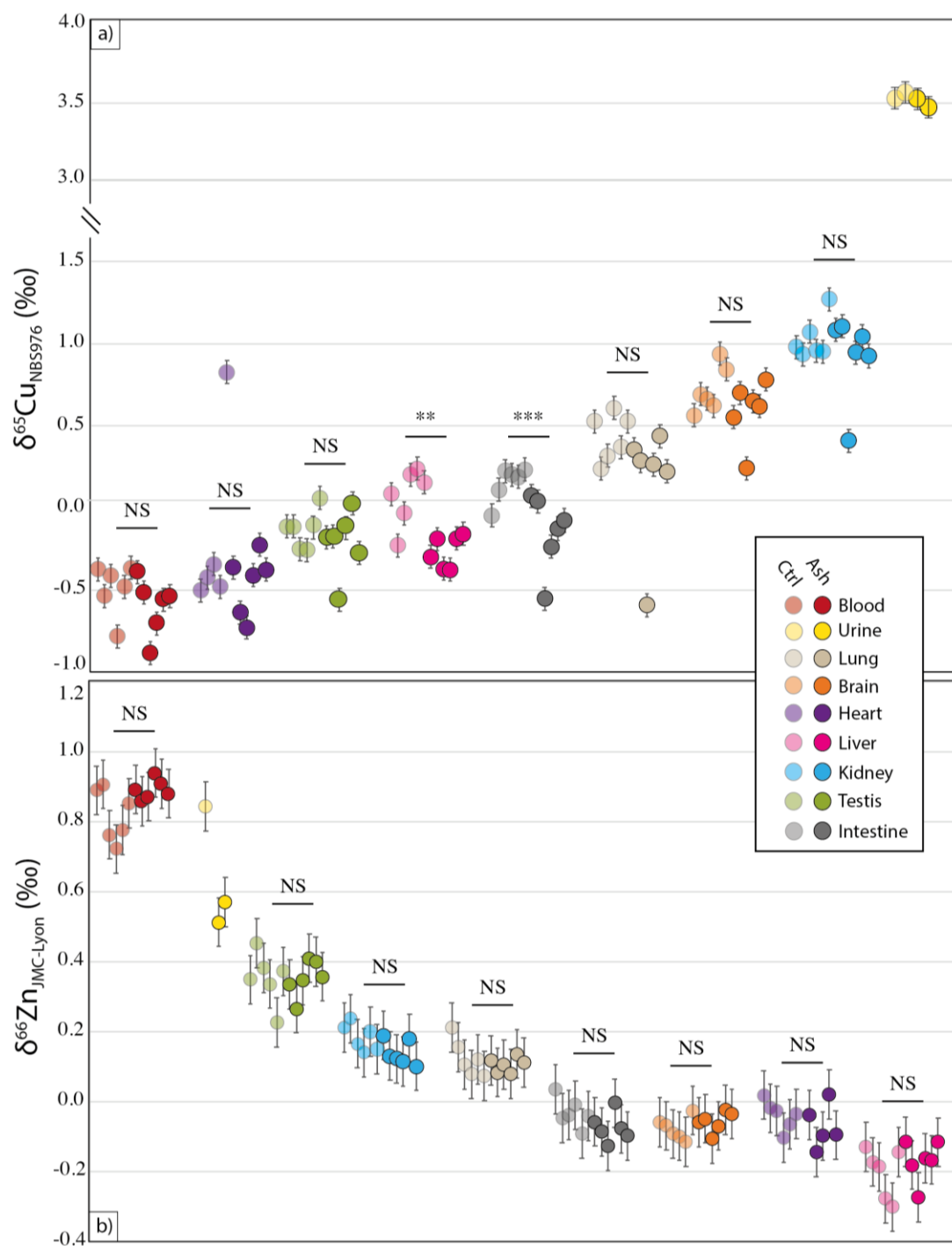


**Figure 3: Copper ( $\delta^{65}\text{Cu}$ ) and zinc ( $\delta^{66}\text{Zn}$ ) isotopic compositions of mice body reservoirs**

Transparency and solid points stand for control and exposed subjects, respectively. For each reservoirs, the approximate  $p$ -value was determined between the control and the exposed group ( $n=6$  per group and per reservoir) by a two-sided non-parametric Mann-Whitney U-test implemented in MATLAB<sup>TM</sup>. \*\* and \*\*\* stand for  $p$ -value lower than 0.02 and 0.01 respectively. For each datapoint, error bars represent 2sd.



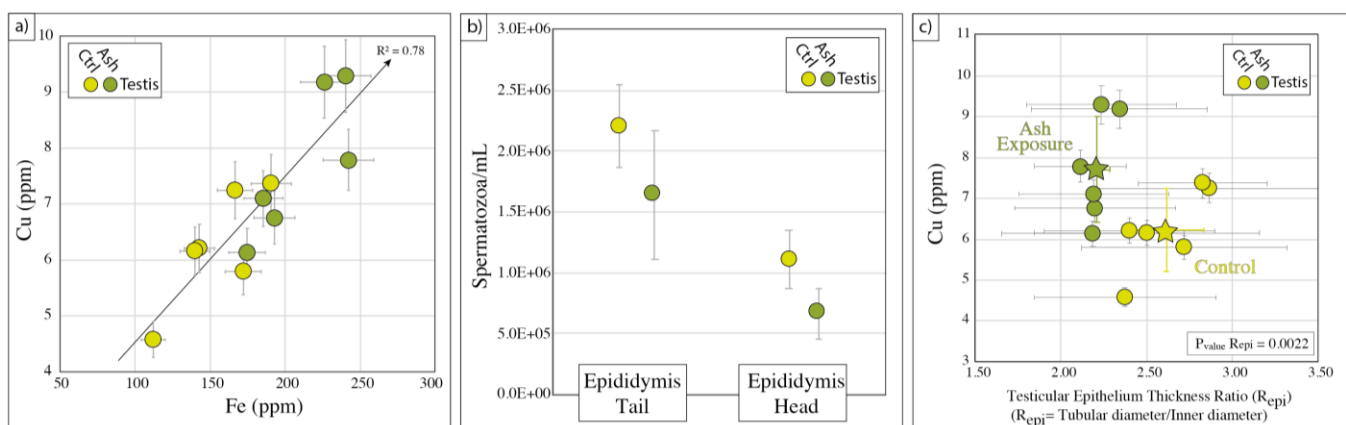


**Figure 4: Volcanic ash-related metallomic and physiological deregulations in testes**

After one month of exposure to metal-rich volcanic ash, mice present (a) testicular copper (Cu) and iron (Fe) accumulation (b) a decrease of the sperm count in the tail and the head of the epididymis and (c) a drop of the testicular epithelium thickness associated to copper increase. Light and dark points stand for control and exposed subjects, respectively. In the left corner diagram (a), for each datapoint, error bars represent 2sd. For the central diagram (b), error bars represent 1sd/ $\sqrt{n}$  with  $n=6$  (i.e. 6 different samples per group from individual mice). Note that for each individual sample, data was obtained on the average of  $n=3$  complete duplicate analyses. For the right corner diagram (c), error bars represent 2sd for Cu concentrations and 1sd for epithelium thickness obtained on the average of  $>20$  seminiferous tubules per sample. Stars stand for the group average and for testicular epithelium thickness, the approximate  $p$ -value was determined by a two-sided non-parametric Mann-Whitney U-test implemented in MATLAB<sup>TM</sup>.

807

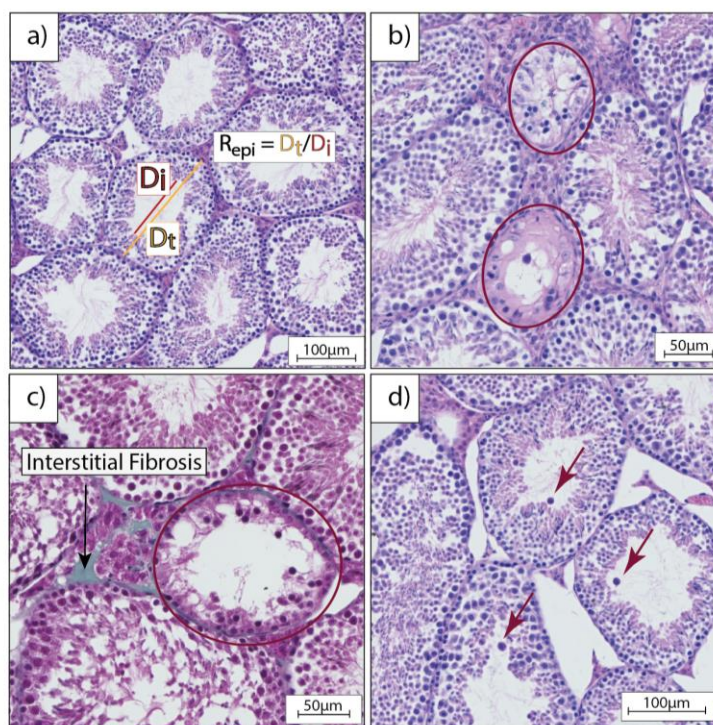


**Figure 5: Histology of mice seminiferous tubules by Hematoxylin/Eosin (HE) and Masson's Trichrome (TM) staining**

Representative micrographs of the testis of (a) control and (b,c and d) mice exposed to volcanic ash. The original magnification was  $\times 20$ . Mice exposed to volcanic ash present germinal epithelium degeneration and tubular vacuolation (b and c) highlighted by red rounded circle, sign of preliminary fibrosis (c) (highlighted by the black arrow and revealed by green coloration with TM staining) and abnormal amount of intratubular atypical germ cells (d) evidenced by the red arrows.

808

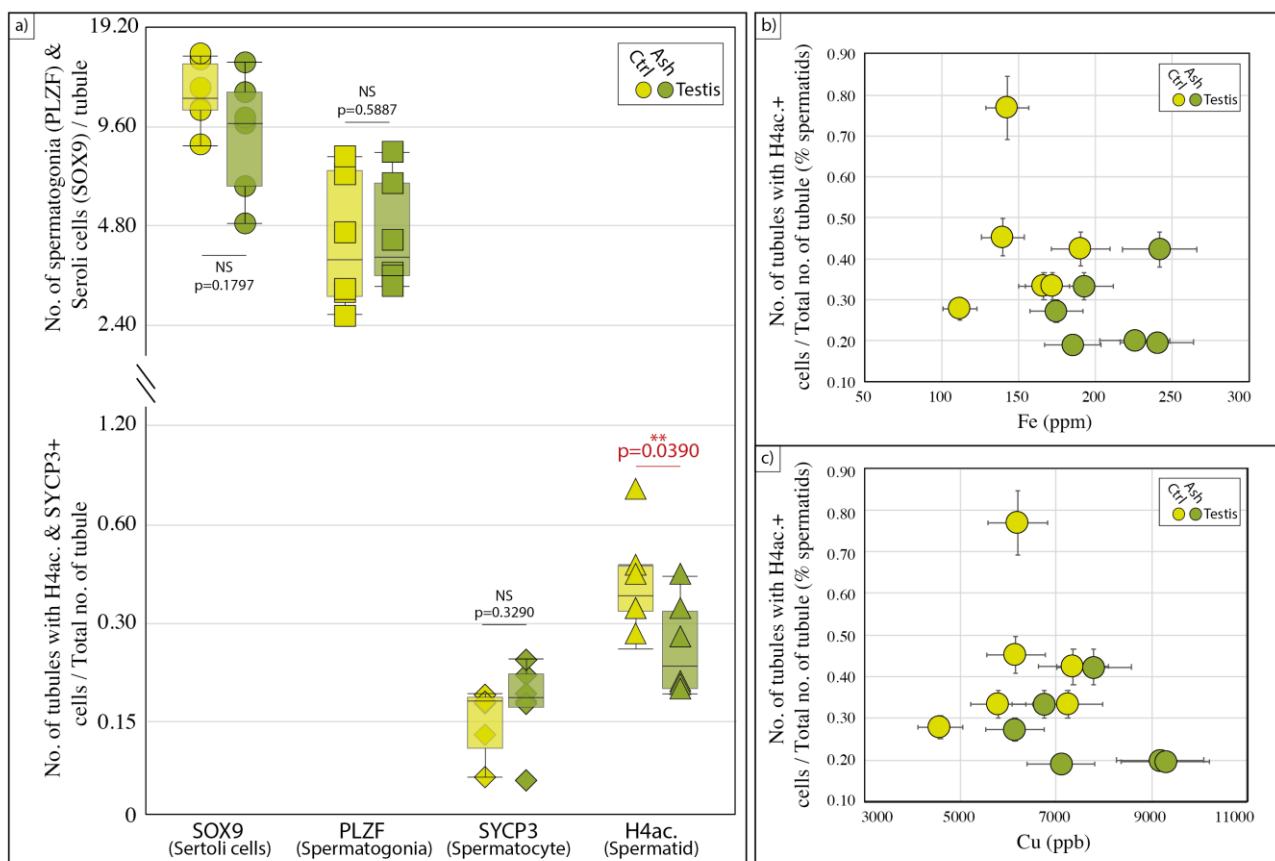


**Figure 6: Immunohistochemical quantification of seminiferous tubules**

(a) Number of normal seminiferous tubules of control and volcanic-ash exposed C57BL/6 males (n=6 per group). Statistical analysis: NS stand for non significant value, \*\* is for  $p < 0.05$  (two-sided non-parametric Mann-Whitney U-test implemented in MATLAB™) (b) & (c) Correlation between the testicular Fe and Cu concentration and the number of acetyl H4+ tubules versus the total number of tubules (n>20). Error bars represent 2sd.

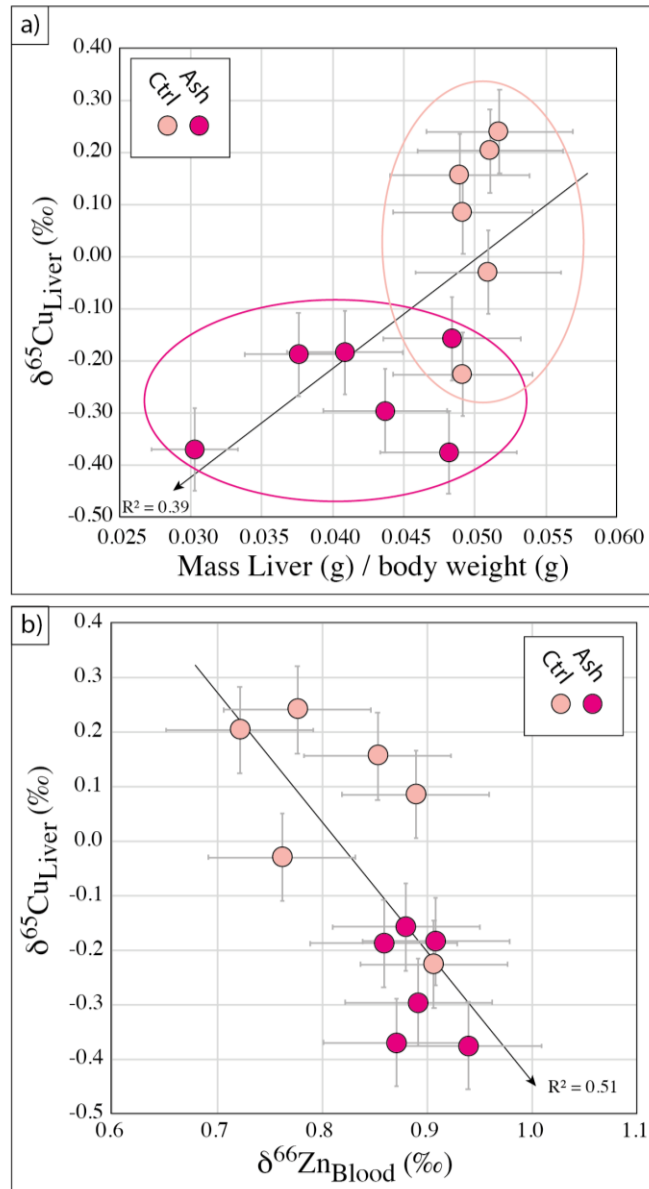


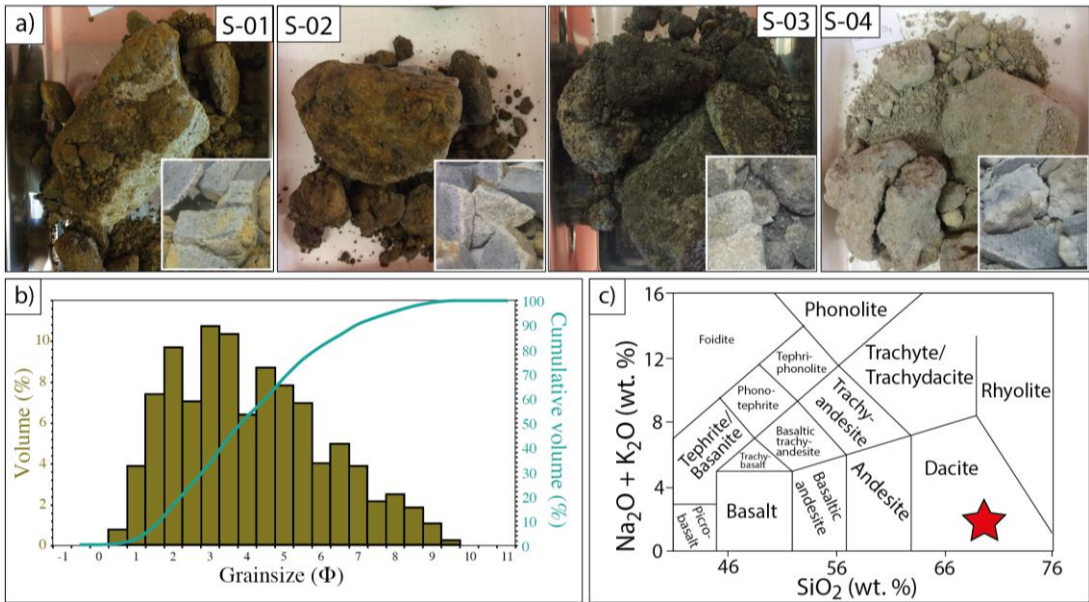
**Figure 7: Volcanic ash-related isotopic and physiological deregulations in liver and blood mice**

Mice exposed to volcanic ash present a significant decrease of the hepatic copper isotopic composition ( $\delta^{65}\text{Cu}$ ) in association with (a) a liver mass loss and (b) a rise of the blood zinc isotopic composition ( $\delta^{66}\text{Zn}$ ). Light and dark points stand for control and exposed subjects, respectively. For each value, analytical error bars represent 2sd.



812  
813

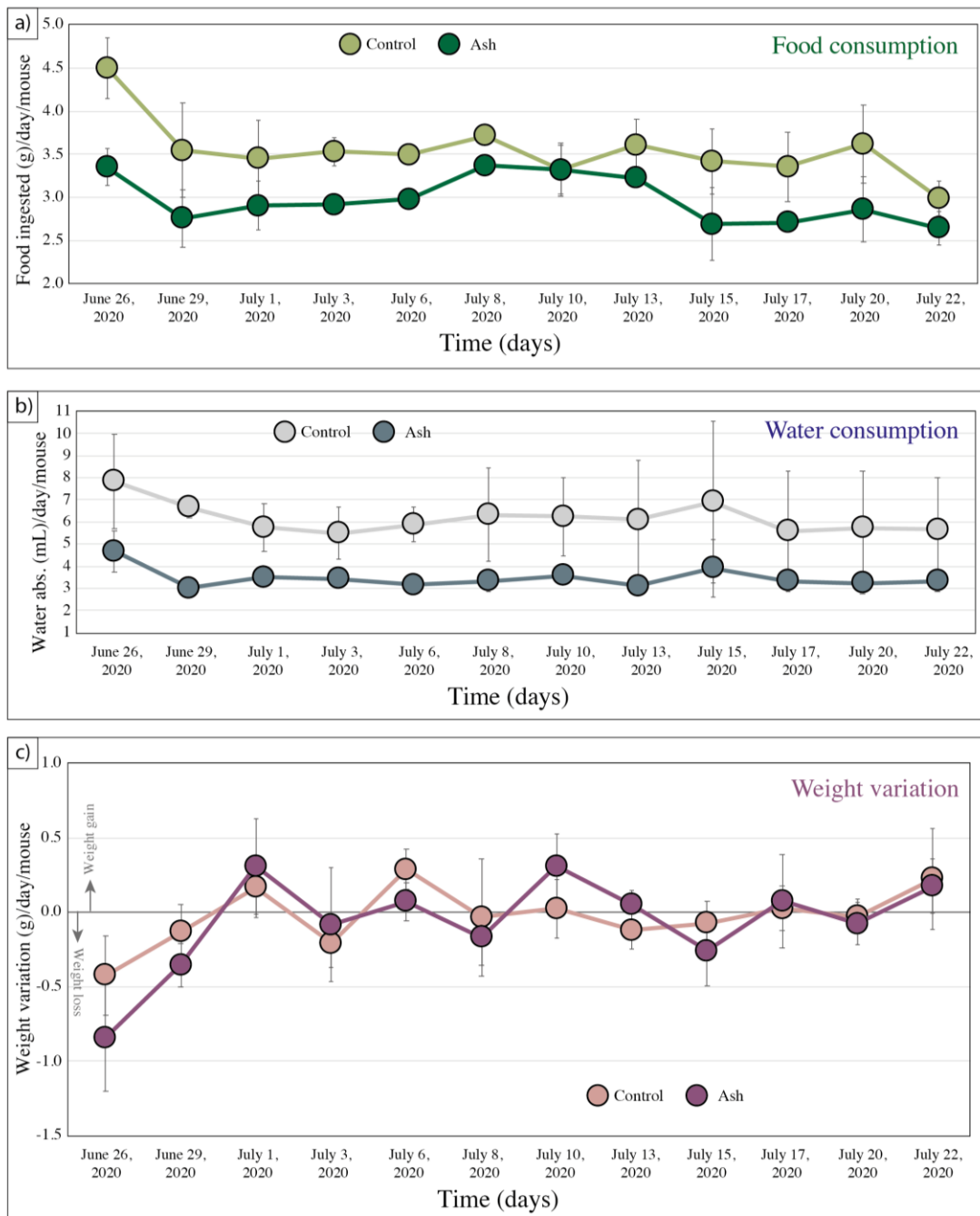
**Supplementary Figures:**



**Supplementary Figure 1: Volcanic sample characterisation**

(a) Visual aspect of the interior and the surface alteration of the four volcanic samples (S-01 to S-04) analyzed in this study, (b) Particle size distribution ( $\Phi = -\log_2(d)$  with  $d$  the diameter of the particle in mm) of the *lab-crushed* volcanic ash sample determined by laser diffraction analyses using a Malvern Mastersizer® analyzer and (c) TAS diagram showing the chemical composition of the volcanic ash sample (red star) as a function of its silica (SiO<sub>2</sub>) and alkaline (Na<sub>2</sub>O+K<sub>2</sub>O) content.

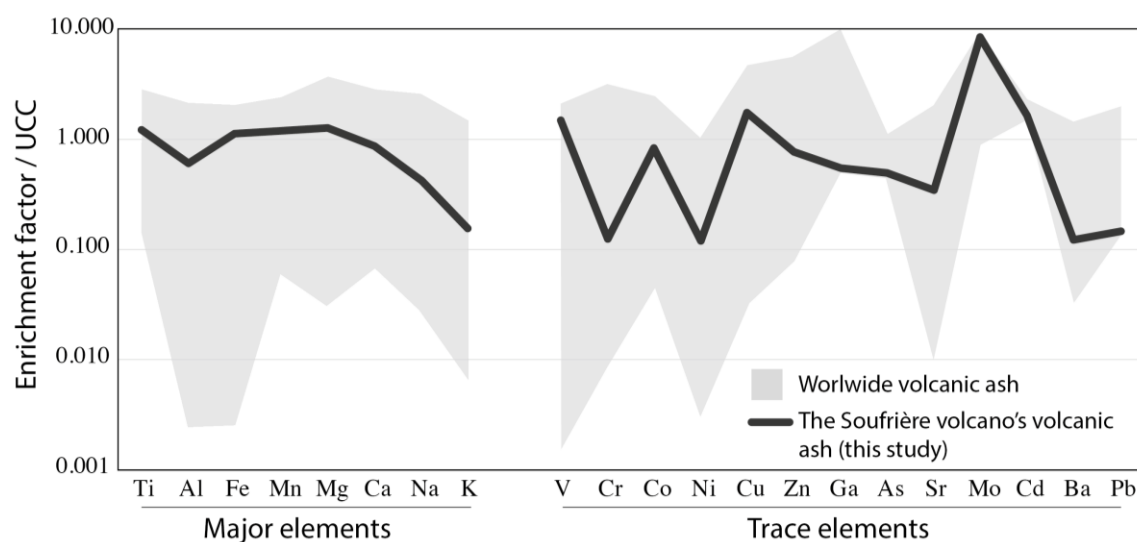
814



**Supplementary Figure 2: Diet and weight variation over time exposure**

Mice exposed over a month to volcanic ash are characterized by (a) Food and (b) Water consumption decrease but (c) no weight variation. Light and dark color point represent control and exposed subjects respectively. For each value, error bars represent 1sd obtained on the average of six data per group (i.e., n=6 mice per group)

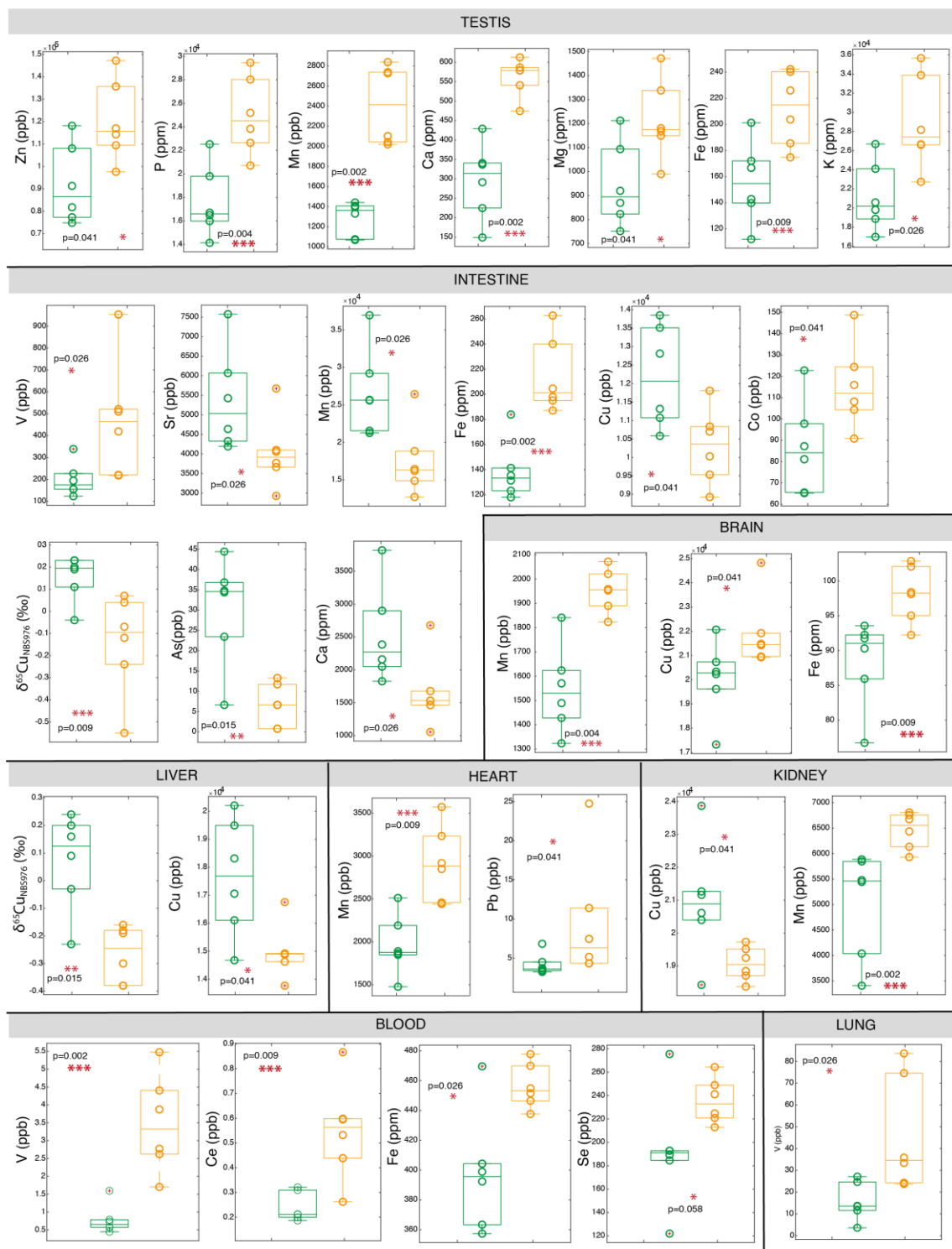
815  
816  
817  
818  
819



**Supplementary Figure 3: Major and trace element patterns of the volcanic ash sample normalized to the upper continental crust (UCC)**

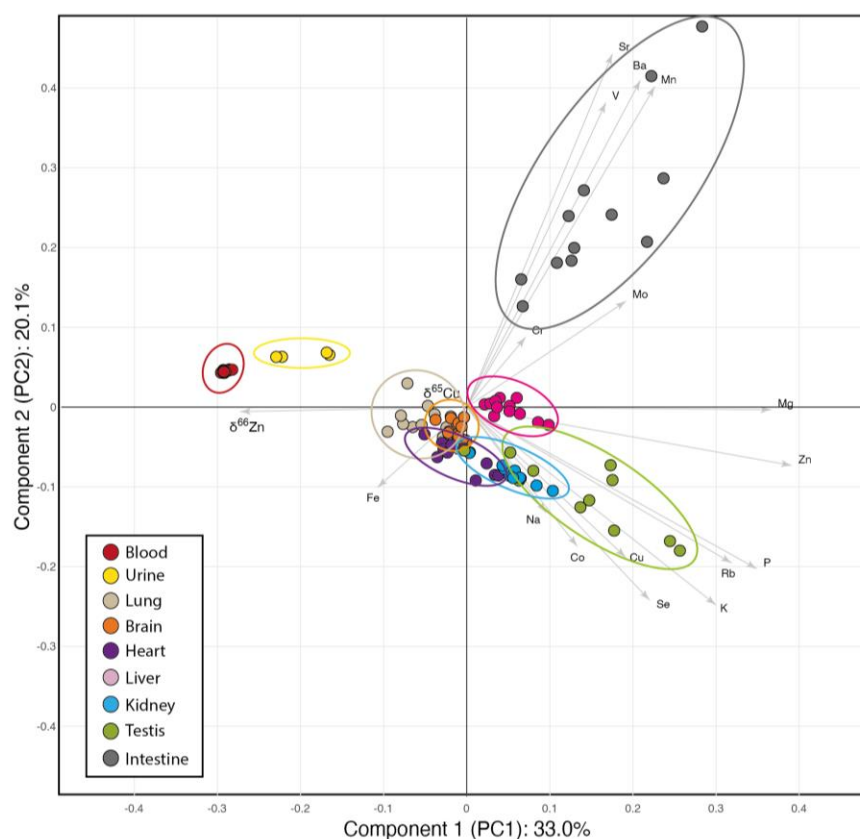
The black line stands for the Soufrière volcanic ash analysed in this study. The grey field represents the average of worlwide volcanic ash obtained on a data compilation from 16 volcanoes/country (Yasur/Vanuatu: Stewart et al., 2006, Córdon Caulle/Chile: Stewart et al., 2016; Eyjafjallajökull/Iceland: Gislason et al., 2011; El Chichón/Mexico: Varekamp et al., 1984; Sinabung/Indonesia: Kusmartini et al., 2017; Puna/Argentina: Ruggieri et al., 2010; Chaitén/Chile: Ruggieri et al., 2012; Shihan/Jordania: Ibrahim et al., 2014; Grímsvötn/Denmark: Lieke et al., 2013; Alpine Anthering/Austria: Huber et al., 2003; Tianchi volcano/China: Ma et al., 2019; Popocatépetl/Mexico: Shruti et al., 2018; Mt Etna/Italy: Toscano et al., 2008; Mt St Helens/USA: Taylor et al., 1980). The average values for the UCC are from Rudnick and Gao, 2014.

820  
821  
822  
823  
824



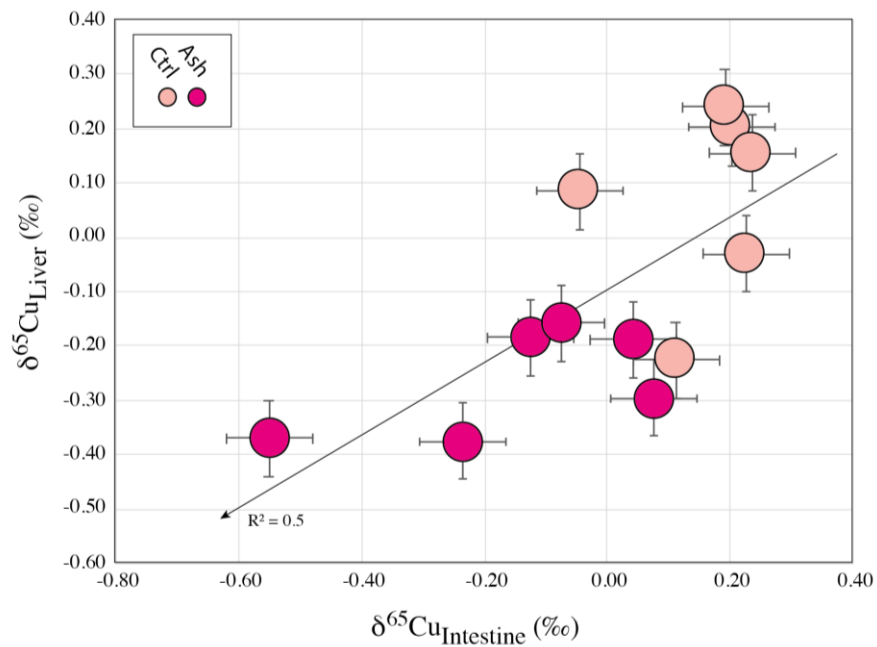
**Supplementary Figure 4: Volcanic ash-related metallome deregulations in mice biological compartments**

Green and yellow points stand for the control and the exposed subjects, respectively. For each diagram, the statistical  $p$ -value was determined between the control and the exposed group ( $n=6$  per group and per reservoir) by a two-sided non-parametric Mann-Whitney U-test implemented in MATLAB™. Only significant  $p$ -value ( $<0.05$ ) are shown with \*, \*\* and \*\*\* standing for  $p$ -value lower than 0.05, 0.02 and 0.01 respectively. With only two points per group, no statistical processing could have been done on the urine reservoir.



#### Supplementary Figure 5: Principal Component Analysis (PCA) of the Results

The PCA allows the classification and the distinction of each mice body reservoirs (organs and body fluids) based on their metallome (i.e., major and trace element and copper, zinc isotopes compositions). In this diagram, all the samples from both the control and the exposed group are represented without any color distinction. The PCA variables include the chemical concentrations of 16 major and trace elements measured in 7 organs and 2 biological fluids of mice, as well as  $\delta^{65}\text{Cu}$  and  $\delta^{66}\text{Zn}$  values. Grey arrow are graphic representations of loading factors in the new PC1 vs. PC2 space. Each body reservoir is distinguishable by a specific color. All data were normalized, and samples with incomplete data were excluded. PCA was implemented in MATLAB™.



**Supplementary Figure 6: Hepatic and intestinal copper isotopic compositions ( $\delta^{65}\text{Cu}$ )**  
Mice exposed to volcanic ash present a significant decrease of the hepatic  $\delta^{65}\text{Cu}$  in association with intestinal  $\delta^{65}\text{Cu}$  drop. Light and dark points stand for control and exposed subjects, respectively. For each value, analytical error bars represent 2sd.

#### Supplementary Tables:

Supplementary Table 1: Geological sampling location				
Sample Name	Sampling date (day/hour)	Longitude	Latitude	Altitude (m)
		UTM coordinate (WGS84)		
S-04	2019-11-18 16:30:36	643041.2877	1774176.37	1453.79
S-03	2019-11-18 16:42:47	643050.5657	1774131.397	1443.32
S-02	2019-11-18 16:54:32	642961.1668	1774222.988	1454.19
S-01	2019-11-18 17:07:48	642955.7651	1774247.627	1442.91

Supplementary Table 2: Major, trace element concentrations and Cu-Zn isotopic composition of biological samples and reference material																									
	Sample Name	V	Cr	Mn	Co	Cu	Zn	As	Se	Rb	Sr	Mo	Cd	Ce	Pb	Ca	Fe	K	Mg	Na	P	$\delta^{65}\text{Cu}_{\text{SM}}$ ‰	$\delta^{66}\text{Zn}_{\text{SM}}$ ‰	Isotope ratio, ‰	
Reference material		Mass fraction, µg/g (ppb)																						Isotope ratio, ‰	
1577c - This study (n=8)	1577c - This study (n=8)	8.67	62.96	9.74E+03	298.13	2.54E+05	1.52E+05	22.52	1811.25	31366.49	108.76	3351.80	91.89	48.81	7.20	61.41	115.18	184.73	9738.16	557.92	1944.94	12107.33	0.27	-0.21	
	2sd	4.92	16.34	2.82E+03	72.16	4.26E+04	3.63E+04	9.10	917.94	6807.34	52.33	910.87	24.97	25.74	2.45	16.21	13.65	39.83	1554.28	96.34	843.52	1867.33	0.08	0.04	
1577c - Certified value	1577c - Certified value	-	53.00	1.05E+04	300.00	2.75E+05	1.81E+05	19.60	2033.00	33000.00	95.00	3300.00	96.57	43.44	-	62.80	133.00	197.94	10230.00	620.00	2033.00	11750.00	0.37	-0.19	
	2sd	-	14.00	4.70E+02	18.00	4.60E+03	1.00E+03	1.40	45.00	13000.00	4.00	1300.00	1.40	13.34	-	1.00	10.00	6.65	6400.00	42.00	64.00	2700.00	0.05	0.05	
Mice Food (n=8)	Mice Food (n=8)	1004.06	1051.89	1.40E+05	194.02	10574.60	81425.34	<LO	184.98	3200.79	18981.45	696.50	113.14	7366.22	-	52.41	12366.60	133.03	4688.27	1896.66	3062.58	8608.24	-0.01	-0.40	
	2sd	63.84	102.12	5.51E+04	55.12	3203.18	5805.64	<LO	25.47	190.76	1394.71	16.86	11.63	721.41	-	6.91	1297.69	1.82	99.65	55.22	729.97	187.47	0.06	0.02	
WHOLE BLOOD	B1	0.57	<LO	88.20	<LO	407.87	3456.07	<LO	<LO	3079.49	28.29	18.77	<LO	5.48	0.21	0.55	36.43	398.88	2262.02	41.24	1572.23	689.61	-0.37	0.88	
	B1 bis	-	-	-	-	-	-	-	-	-	-	-	-	-	-	-	-	-	-	-	-	-	-	-	
	B2	0.45	<LO	51.21	<LO	419.53	3556.07	<LO	<LO	189.25	3024.47	26.36	15.91	<LO	0.21	0.46	40.59	392.35	2307.79	37.78	1742.90	679.58	-0.54	0.91	
	B2 bis	<LO	<LO	48.94	<LO	453.28	3842.54	<LO	<LO	179.16	3235.58	28.36	19.04	<LO	1.56	0.28	0.59	42.78	42.75	-	-	-	-	-	
	B3	1.59	4.06	52.22	3.33	450.86	4051.80	<LO	<LO	324.99	3271.02	25.54	18.95	<LO	1.46	0.31	0.34	48.54	404.32	2285.79	42.87	1636.85	707.39	-0.41	0.76
	B4	0.73	<LO	53.51	<LO	612.30	3380.65	<LO	<LO	<LO	3137.52	30.40	16.17	<LO	1.34	0.20	0.54	49.56	363.39	2093.82	43.25	1913.80	704.40	-0.81	0.72
	B4 bis	-	-	-	-	-	-	-	-	-	-	-	-	-	-	-	-	-	-	-	-	-	-	-	
	B5	0.57	<LO	48.93	<LO	602.08	3412.09	<LO	<LO	184.55	2890.22	29.60	15.55	<LO	<LO	0.19	0.32	48.20	357.39	2012.60	42.69	1884.38	693.32	-0.49	0.78
	B5 bis	-	-	-	-	-	-	-	-	-	-	-	-	-	-	-	-	-	-	-	-	-	-	-	
	B6	<LO	<LO	69.59	<LO	449.75	3940.83	<LO	<LO	275.42	2714.85	35.80	21.55	<LO	<LO	0.32	-	47.03	469.58	2583.12	44.00	1672.89	770.32	-0.36	0.85
	B7	3.87	<LO	78.75	<LO	517.54	4220.38	<LO	<LO	220.87	2898.79	38.95	19.45	<LO	4.76	0.53	0.43	44.09	477.81	2378.91	47.06	1535.04	728.57	-0.39	0.89
	B8	4.40	4.84	70.72	<LO	478.70	3978.12	<LO	<LO	224.67	3156.71	31.34	16.93	<LO	3.74	0.60	0.61	43.44	451.55	2319.49	43.76	1652.94	718.98	-0.52	0.86
	B9	5.49	8.69	86.55	<LO	582.83	3788.13	<LO	<LO	264.34	3458.83	32.11	21.74	<LO	4.01	0.60	0.50	45.56	454.85	2470.61	44.26	1600.03	735.62	-0.67	0.87
	B10	6.67	3.82	87.24	<LO	600.18	3826.95	<LO	<LO	230.48	3473.65	31.31	21.44	<LO	4.38	0.52	0.43	-	467.09	-	46.94	-	-	-	-
	B10 bis	1.70	<LO	55.83	<LO	477.03	4110.17	<LO	<LO	241.10	3050.45	31.21	13.69	<LO	2.27	0.26	0.36	45.53	469.93	2491.27	42.24	1650.88	767.15	-0.70	0.91
	B11	2.77	5.44	72.09	<LO	430.44	3755.13	<LO	<LO	248.89	3156.06	34.11	17.36	<LO	3.05	0.87	0.43	47.82	446.46	2458.95	42.08	1670.39	768.06	-0.56	0.91
	B12	2.62	<LO	60.63	<LO	424.98	3937.63	<LO	<LO	212.91	3153.85	26.33	15.32	<LO	1.84	0.44	0.43	48.86	437.63	2354.10	42.59	1731.74	709.13	-0.54	0.88
URINE	Ua ctrl	1.43	<LO	25.26	6.62	143.88	142.66	32.88	<LO	<LO	4167.35	71.87	40.77	<LO	33.31	0.31	0.49	339.56	0.18	5528.57	725.33	2292.41	38.20	34.9	0.84
	Ub ctrl	<LO	<LO	<LO	<LO	<LO	<LO	<LO	<LO	3688.55	587.99	554.82	<LO	50.19	2.32	4.84	116.27	<LO	6589.26	565.67	1738.69	363.76	3.53	-	-
	Uc ctrl	<LO	<LO	<LO	<LO	<LO	<LO	<LO	<LO	3712.91	569.08	581.76	<LO	42.56	2.56	<LO	-	-	-	-	-	-	-	-	-
	Ud ash	13.57	<LO	183.93	<LO	98.47	241.39	65.94	<LO	5480.58	877.06	605.69	<LO	55.79	2.33	1.98	256.28	4.67	8211.86	1158.95	2331.79	63.36	34.9	0.51	
TESTES	Ud ash	21.07	7.91	94.45	9.31	122.18	149.18	45.91	246.72	4292.45	1019.15	445.58	<LO	52.15	1.55	1.28	541.56	4.04	6000.26	1230.27	3600.95	45.63	34.9	0.51	
	T1	42.04	1853.62	1330.98	159.53	6205.51	8.18E+04	126.26	6234.70	40925.09	147.05	633.06	<LO	159.66	9.15	16.88	149.11	142.84	16399.74	869.51	-	14134.01	-1.11	0.35	
	T2	14.30	1271.85	1068.12	146.28	6156.71	9.13E+04	99.94	5454.05	43688.31	66.38	343.53	<LO	64.18	3.72	17.64	224.68	139.77	19813.75	919.67	-	16695.28	-1.11	0.45	
	T3	39.03	590.81	1407.35	188.68	7247.08	1.08E+05	107.76	6898.22	53354.35	162.35	394.52	<LO	82.45	6.11	21.20	291.21	166.67	24101.98	1093.52	-	17999.52	-0.25	0.38	
	T4	28.13	1084.93	1443.39	200.91	8081.68	1.18E+05	143.04	7670.07	59421.58	194.68	387.74	<LO	92.44	8.49	31.13	340.54	201.23	26687.14	1212.31	-	22523.97	-0.26	0.34	
	T5	27.09	962.61	1293.76	184.72	6647.68	1.07E+05	107.76	6898.22	53354.35	162.35	394.52	<LO	82.45	6.11	21.20	291.21	166.67	24101.98	1093.52	-	17999.52	-0.25	0.38	
	T5	34.92	169.07	1075.94	176.34	5792.18	7.73E+04	98.75	6629.32	39564.88	149.85	248.41	<LO	185.64	7.18	18.56	336.67	172.11	18874.38	823.03	-	15979.72	-0.10	0.23	
	T6	10.78	116.87	1393.85	120.93	4578.38	7.48E+04	10.61	5613.07	30736.36	104.11	164.50	<LO	66.60	3.69	15.55	428.73	112.11	20993.21	751.58	-	16486.37	0.06	0.37	
	T7	25.40	1942.93	2356.41	207.22	9198.47	1.36E+05	123.36	9101.22	5871.76	268.85	444.66	<LO	122.52	7.94	28.68	612.49	226.00	33878.89	1337.92	-	28025.84	0.18	0.33	
	T8	62.91	441.73	2101.84	231.85	7780.60	1.09E+05	93.20	8505.27	53130.04	941.70	346.45	<LO	263.83	33.73	48.97	540.78	242.38	26664.79	1148.41	-	22641.93	-0.17	0.27	
	T9	82.04	226.73	2888.17	207.72	7304.09	1.17E+05	61.23	6241.62	58008.67	427.22	245.78	<LO	670.01	11.49	25.87	578.23	203.75	26605.08	1180.48	-	23811.12	-0.56	0.35	
	T9 bis	40.15	193.29	2415.85	179.20	6213.42	1.05E+05	<LO	<LO	4817.03	322.32	161.61	<LO	522.63	10.41	21.05	-	182.05	-	-	-	-	-	-	-
	T10	35.28	262.33	2737.99	238.45	9290.33	1.47E+05	73.05	8269.37	66419.42	138.36	417.29	<LO	85.30	6.09	29.08	578.94	240.33	35658.75	1471.67	-	24562.71	-0.12	0.39	
	T10 bis	-	-	-	-	-	-	-	-	-	-	-	-	-	-	-	-	-	-	-	-	-	-	-	
	T11	60.13	527.65	2042.83	167.72	6137.82	9.76E+04	27.64	5000.14	43095.04	129.68	260.41	<LO	91.72	7.01	15.50	474.39	174.77	22744.42	989.48	-	20909.06	0.03	0.40	
	T12	44.48	358.86	2059.12	175.45	7104.83	1.14E+05	27.68	6026.73	54699.56	103.48	301.73	<LO	82.90	3.52	17.01	586.34	186.49	28188.55	1168.61	-	25139.16	-0.27	0.36	
	U1	27.10	944.35	1087.65	56.18	12624.56	33588.98	80.78	2062.15	26069.67	61.86	1237.30	11.92	114.98	<LO	7.02	<LO	915.58	10428.85	434.43	6258.38	968.64	0.53	0.21	
	U1 bis	52.28	10706.88	1142.19	55.15	12524.87	37579.28	63.75	1606.15	27537.86	66.80	1345.91	11.54	119.74	<LO	1.41	<LO	1013.47	-	-	-	-	-	-	
	U2	13.53	683.17	100.55	10.05	1129.58	100.00	10.00	10.00	10.00	10.00	10.00	10.00	10.00	10.00	10.00	10.00	10							



Supplementary Table 3: Food ingested, water absorbed and weight variation over time exposure												
	Food ingested (g) / day / mouse				Water absorbed (mL) / day / mouse				Weight variation (g) / day / mouse			
Measurement Date	Control Group (n=6)	1 $\sigma$ (n=6)	Exposed group (n=6)	1 $\sigma$ (n=6)	Control Group (n=6)	1 $\sigma$ (n=6)	Exposed group (n=6)	1 $\sigma$ (n=6)	Control Group (n=6)	1 $\sigma$ (n=6)	Exposed group (n=6)	1 $\sigma$ (n=6)
2020-06-26	4.5	0.4	3.4	0.2	7.8	2.1	4.7	0.9	-0.4	0.3	-0.8	0.4
2020-06-29	3.5	0.5	2.8	0.3	6.7	0.5	3.0	0.2	-0.1	0.2	-0.4	0.1
2020-07-01	3.5	0.4	2.9	0.3	5.8	1.1	3.5	0.2	0.2	0.2	0.3	0.3
2020-07-03	3.5	0.2	2.9	0.1	5.5	1.2	3.4	0.1	-0.2	0.2	-0.1	0.4
2020-07-06	3.5	0.0	3.0	0.0	5.9	0.8	3.2	0.4	0.3	0.1	0.1	0.1
2020-07-08	3.7	0.1	3.4	0.1	6.3	2.1	3.3	0.5	0.0	0.4	-0.2	0.2
2020-07-10	3.3	0.3	3.3	0.3	6.3	1.8	3.6	0.4	0.0	0.2	0.3	0.2
2020-07-13	3.6	0.3	3.2	0.1	6.1	2.7	3.1	0.3	-0.1	0.1	0.0	0.1
2020-07-15	3.4	0.4	2.7	0.4	6.9	3.7	3.9	1.3	-0.1	0.2	-0.3	0.2
2020-07-17	3.4	0.4	2.7	0.1	5.6	2.7	3.3	0.0	0.0	0.2	0.1	0.3
2020-07-20	3.6	0.5	2.9	0.4	5.7	2.6	3.2	0.5	0.0	0.1	-0.1	0.1
2020-07-22	3.0	0.2	2.6	0.2	5.7	2.4	3.3	0.5	0.2	0.3	0.2	0.2

837  
838

**Supplementary Table 4:** Mass of the entire organ (wet weight i.e., before freeze-drying) normalised to body weight at sacrifice date

	Sample Name	Mass organ (g) / Body weight (g)					
TESTIS	T1	0.0058					
	T2	0.0059					
	T3	0.0062					
	T4	0.0056					
	T5	0.0046					
	T6	0.0069					
	T7	0.0067					
	T8	0.0048					
	T9	0.0062					
	T10	0.0067					
	T11	0.0065					
	T12	0.0068					
LUNG	Lu1	0.0065					
	Lu2	0.0048					
	Lu3	0.0052					
	Lu4	0.0047					
	Lu5	0.0064					
	Lu6	0.0044					
	Lu7	0.0050					
	Lu8	0.0052					
	Lu9	0.0048					
	Lu10	0.0064					
	Lu11	0.0045					
	Lu12	0.0053					
INTESTINE	I1	0.0370					
	I2	0.0322					
	I3	0.0241					
	I4	0.0315					
	I5	0.0287					
	I6	0.0263					
	I7	0.0316					
	I8	0.0272					
	I9	0.0304					
	I10	0.0311					
	I11	0.0275					
	I12	0.0246					
BRAIN	Br1	0.0132					
	Br2	0.0133					
	Br3	0.0132					
	Br4	0.0127					
	Br5	0.0138					
	Br6	0.0156					
	Br7	0.0146					
	Br8	0.0138					
	Br9	0.0149					
	Br10	0.0148					
	Br11	0.0139					
	Br12	0.0137					
LIVER	Liv1	0.0492					
	Liv2	0.0492					
	Liv3	0.0510					
	Liv4	0.0511					
	Liv5	0.0517					
	Liv6	0.0489					
	Liv7	0.0437					
	Liv8	0.0376					
	Liv9	0.0303					
	Liv10	0.0482					
	Liv11	0.0408					
	Liv12	0.0484					
HEART	H1	0.0055					
	H2	0.0056					
	H3	0.0060					
	H4	0.0054					
	H5	0.0052					
	H6	0.0049					
	H7	0.0042					
	H8	0.0051					
	H9	0.0054					
	H10	0.0045					
	H11	0.0042					
	H12	0.0046					
KIDNEY	K1	0.0102					
	K2	0.0108					
	K3	0.0119					
	K4	0.0118					
	K5	0.0116					
	K6	0.0120					
	K7	0.0117					
	K8	0.0110					
	K9	0.0132					
	K10	0.0124					
	K11	0.0101					
	K12	0.0099					

**Table caption:** Sample ID from 1 to 6 stand for control mice and from 7 to 12 for mice exposed to volcanic ash over one month

**Supplementary Table 5:** Spermatozoa count in the tail and the head of epididymis of C57BL/6 control (ID: 1 to 6) and exposed mice (ID: 7 to 12) to volcanic ash

	Mice ID	Sperm count / mL (n=3)	$\sigma/Vn$ (n=3)	Average Sperm count / mL (n=6)	$\sigma/Vn$ (n=6)								
Epididymis Tail	1	2.1E+06	2.9E+05	2.21E+06	3.42E+05								
	2	1.2E+06	1.6E+05										
	3	2.7E+06	8.4E+05										
	4	1.6E+06	2.0E+04										
	5	3.5E+06	9.6E+05										
	6	2.3E+06	0.0E+00										
	7	1.1E+06	3.7E+05	1.64E+06	5.32E+05								
	8	1.1E+06	2.0E+04										
	9	3.6E+06	7.8E+05										
	10	6.3E+05	6.1E+04										
	11	4.8E+05	2.0E+04										
	12	3.0E+06	7.6E+05										
Epididymis Head	1	1.9E+06	6.9E+05	1.11E+06	2.36E+05								
	2	5.5E+05	0.0E+00										
	3	1.6E+06	1.0E+05										
	4	5.0E+05	1.6E+05										
	5	8.3E+05	3.9E+05										
	6	1.3E+06	0.0E+00										
	7	5.0E+05	2.0E+05	6.63E+05	2.07E+05								
	8	2.0E+05	4.1E+04										
	9	4.3E+05	2.0E+04										
	10	6.5E+05	2.4E+05										
	11	1.7E+06	3.7E+05										
	12	5.5E+05	4.1E+04										

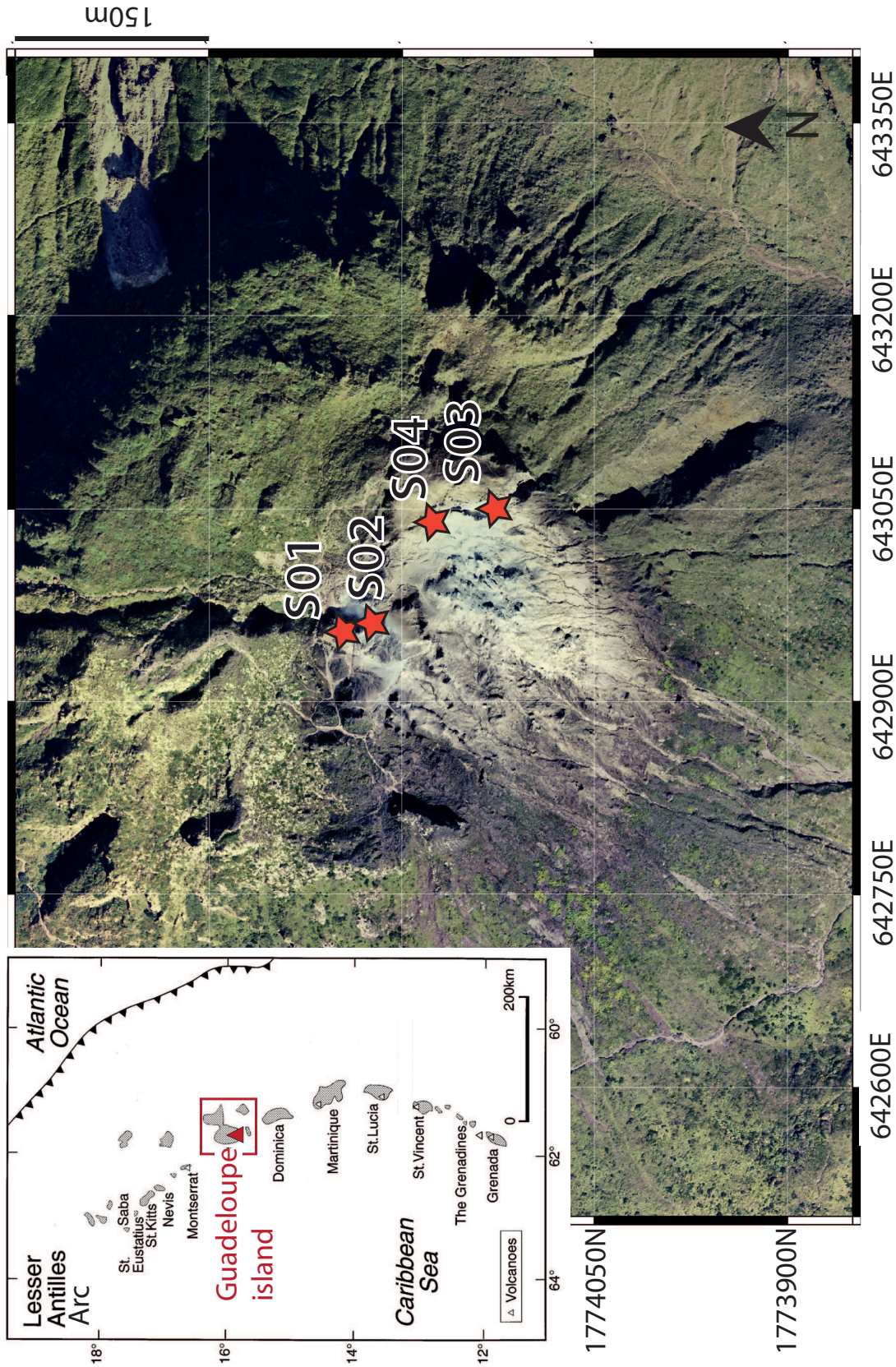
**Supplementary Table 6:** Testicular epithelium thickness ratio & Immunohistochemical quantification

Testicular epithelium thickness			Immunohistochemical quantification			
Sample Name	R <sub>epi</sub> (Testicular Epithelium Thickness Ratio)	1 $\sigma$ (n=20)	No. of acetyl-Histone H4+ tubule/total tubule	No. of SYCP3+ tubule/total tubule	No. of PLZF+ cells/tubule (n>20)	No. of SOX9+ cells/tubule (n>20)
T1	2.44	0.65	0.77	0.17	2.55	10.72
T2	2.78	0.74	0.45	0.18	2.98	10.59
T3	3.17	0.77	0.33	0.08	6.82	15.09
T4	2.82	0.44	0.42	-	7.69	12.40
T5	2.57	0.40	0.33	0.17	3.05	15.82
T6	2.43	0.38	0.28	0.12	4.54	8.33
T7	2.07	0.47	0.20	0.17	7.93	9.73
T8	2.10	0.27	0.42	0.21	3.42	12.05
T9	1.98	0.23	0.33	0.19	3.35	6.28
T10	2.17	0.36	0.20	0.24	6.39	10.13
T11	2.07	0.39	0.27	0.05	3.11	4.81
T12	2.05	0.33	0.19	0.17	4.32	14.80

**Table caption:** Sample from T1 to T6 stand for control mice and from T7 to T12 for mice exposed to volcanic ash over one month

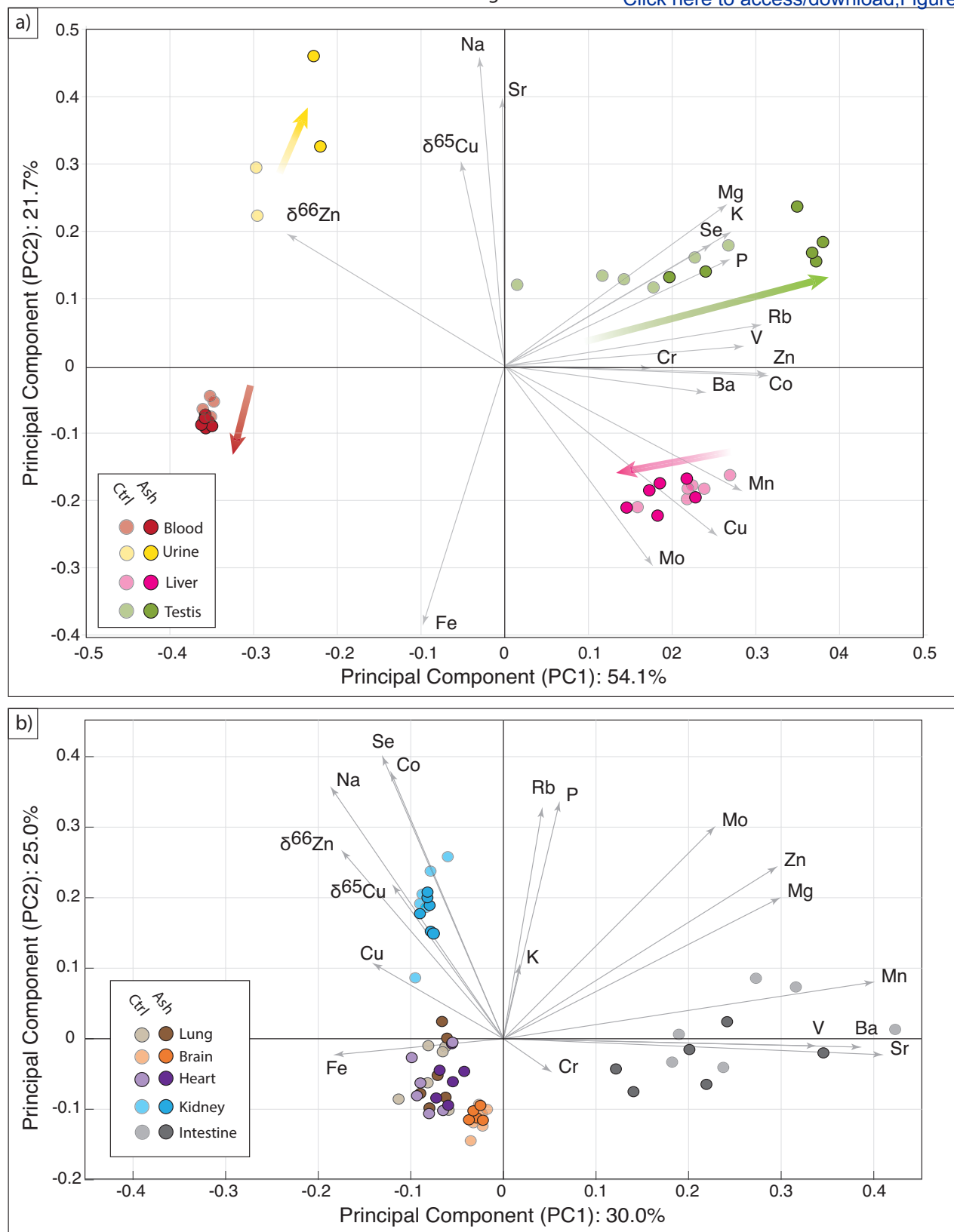
**Table caption:** n stands for complete duplicate analysis  
<LD stand for lower limit of detection calculated following  
"-" stand for not measured sample

Figure 1



**Figure 1: Location map of the studied area**

Map of the Soufrière volcano located in the Guadeloupe island (Basse-Terre) of the Lesser Antilles arc (UTM coordinates). The red triangle indicate the location of the Soufrière volcano and the red stars indicate the sampling locations of the rocks from the volcanic dome (S01 to S04) used to reproduce «artificial» volcanic ash later exposed to mice in this study. S01 and S02 were collected on the «Tarissan» site while S03 and S04 are from the «Cratère Sud» site.



**Figure 2. Principal Component Analysis (PCA) of the Results**

The PCA allows (a) the identification of organs (i.e. testis and liver) and body fluids (i.e. blood and urine) preferentially affected by metallome deregulation (i.e. metallome difference between control and exposed subjects) due to volcanic ash exposure from (b) those that are less (i.e. no metallome difference between control and exposed subjects). In this study, the variables include the chemical concentrations of 16 major and trace elements measured in 7 organs and 2 biological fluids of mice, as well as  $\delta^{65}\text{Cu}$  and  $\delta^{66}\text{Zn}$  values. Grey arrows are graphic representations of loading factors in the new PC1 vs. PC2 space. The coordinates of each sample in the new PC1 vs. PC2 space (i.e. sample scores) are shown by circles. Transparency and solid points stand for control and exposed subjects, respectively. All data were normalized, and samples with incomplete data were excluded. PCA was implemented in MATLAB™.



Figure 3

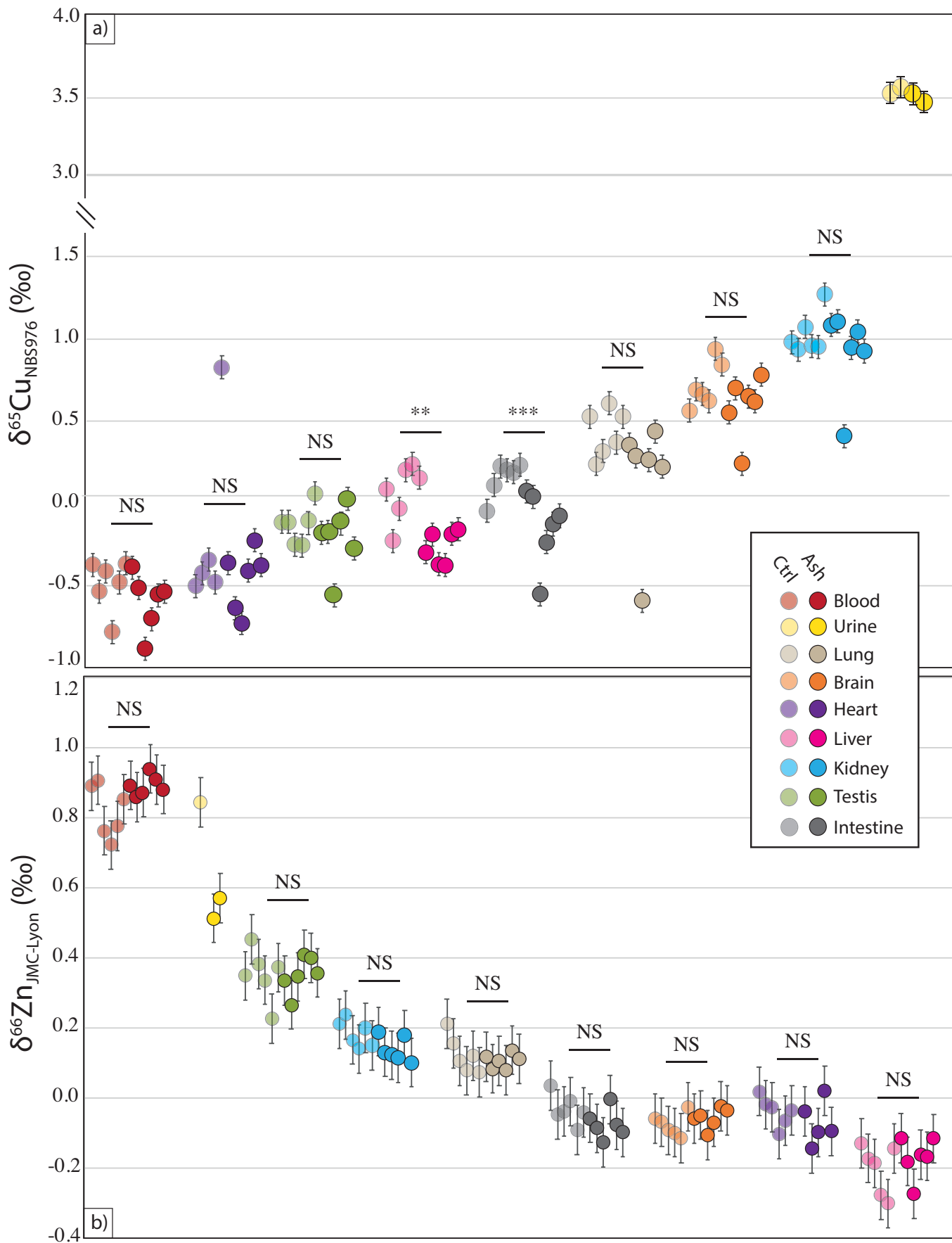
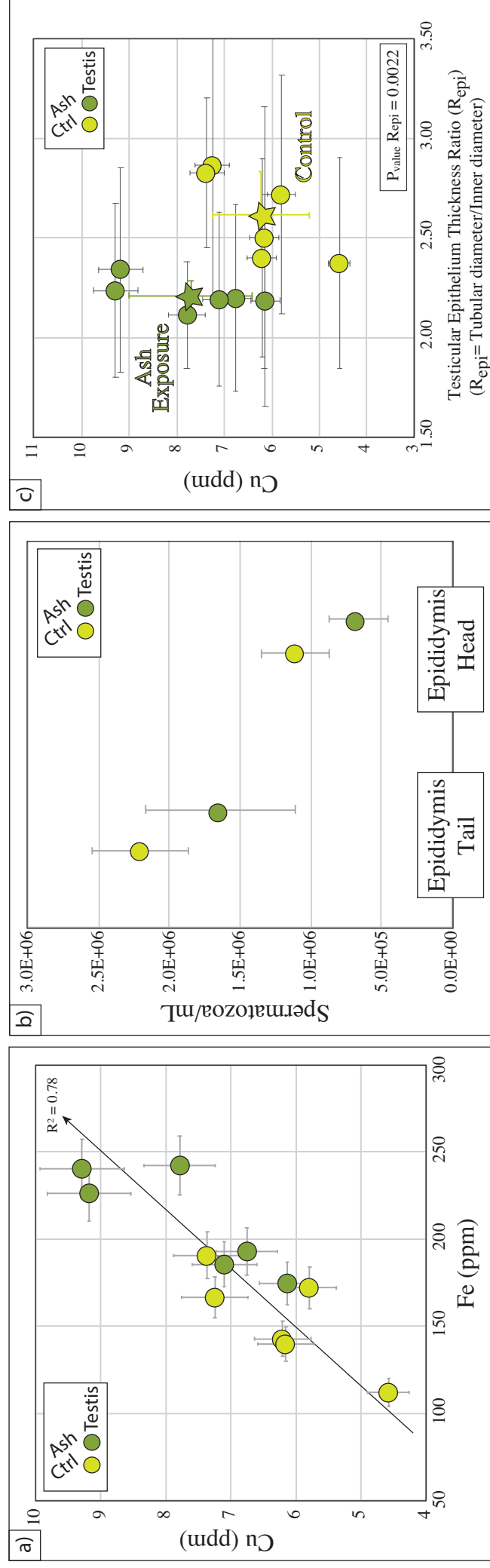
[Click here to access/download;Figure;Figure3.eps](#)


Figure 4



**Figure 4: Volcanic ash-related metallomic and physiological deregulations in testes**

After one month of exposure to metal-rich volcanic ash, mice present (a) testicular copper (Cu) and iron (Fe) accumulation

(b) a decrease of the sperm count in the tail and the head of the epididymis and (c) a drop of the testicular epithelium thickness associated to copper increase. Light and dark points stand for control and exposed subjects, respectively. In the left corner diagram (a), for each datapoint, error bars represent 2sd. For the central diagram (b), error bars represent 1sd/ $\sqrt{n}$  with  $n=6$  (i.e. 6 different samples per group from individual mice). Note that for each individual sample, data was obtained on the average of  $n=3$  complete duplicate analyses. For the right corner diagram (c), error bars represent 2sd for Cu concentrations and 1sd for epithelium thickness obtained on the average of  $>20$  seminiferous tubules per sample. Stars stand for the group average and for testicular epithelium thickness, the approximate  $p$ -value was determined by a two-sided non-parametric Mann-Whitney U-test implemented in MATLAB<sup>TM</sup>.



**Figure 5**

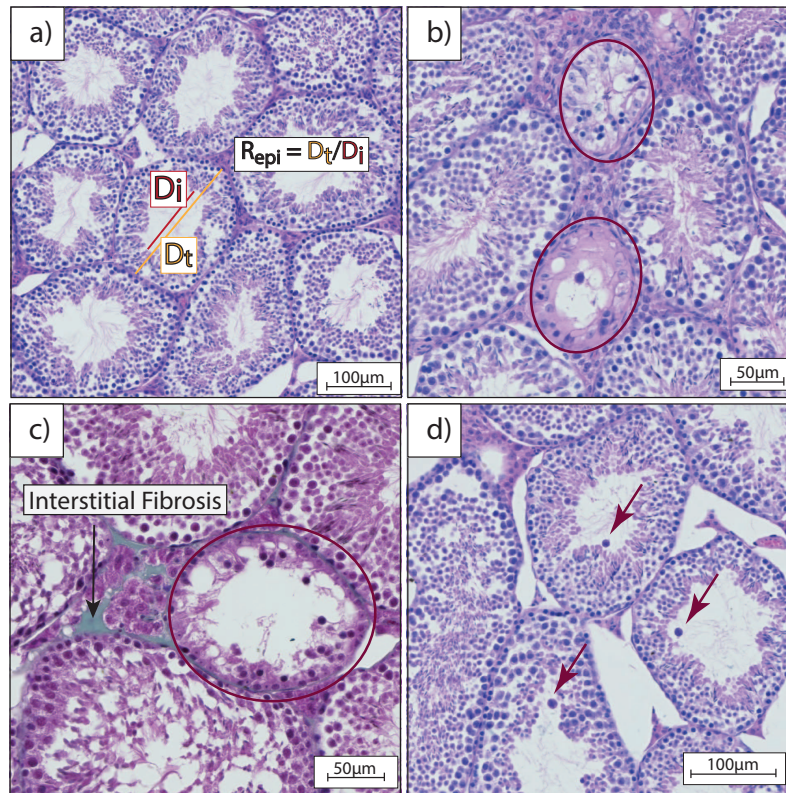


**Figure 5: Histology of mice seminiferous tubules by Hematoxylin/Eosin (HE) and Masson's Trichrome (TM) staining**

Representative micrographs of the testis of (a) control and (b,c and d) mice exposed to volcanic ash. The original magnification was x20. Mice exposed to volcanic ash present germinal epithelium degeneration and tubular vacuolation (b and c) highlighted by red rounded circle, sign of preliminary fibrosis (c) (highlighted by the black arrow and revealed by green coloration with TM staining) and abnormal amount of intratubular atypical germ cells (d) evidenced by the red arrows.

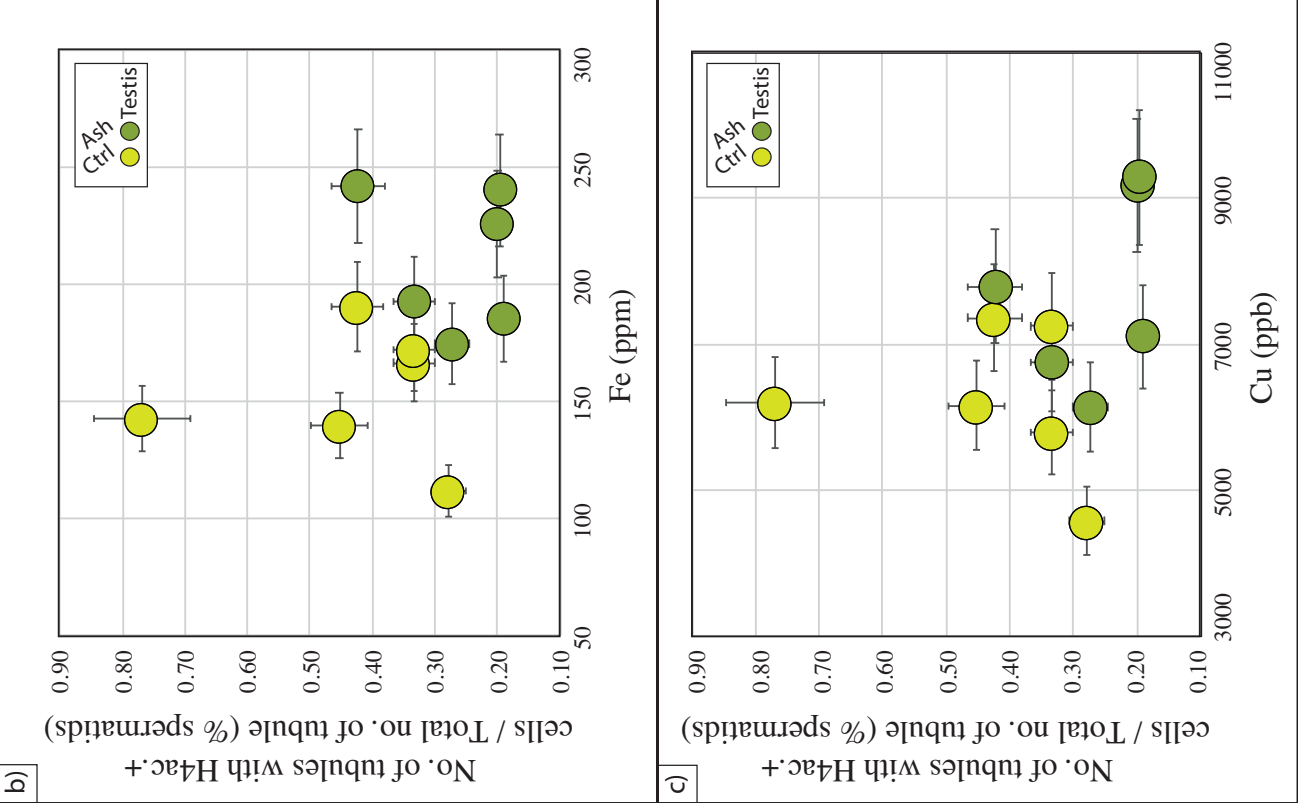
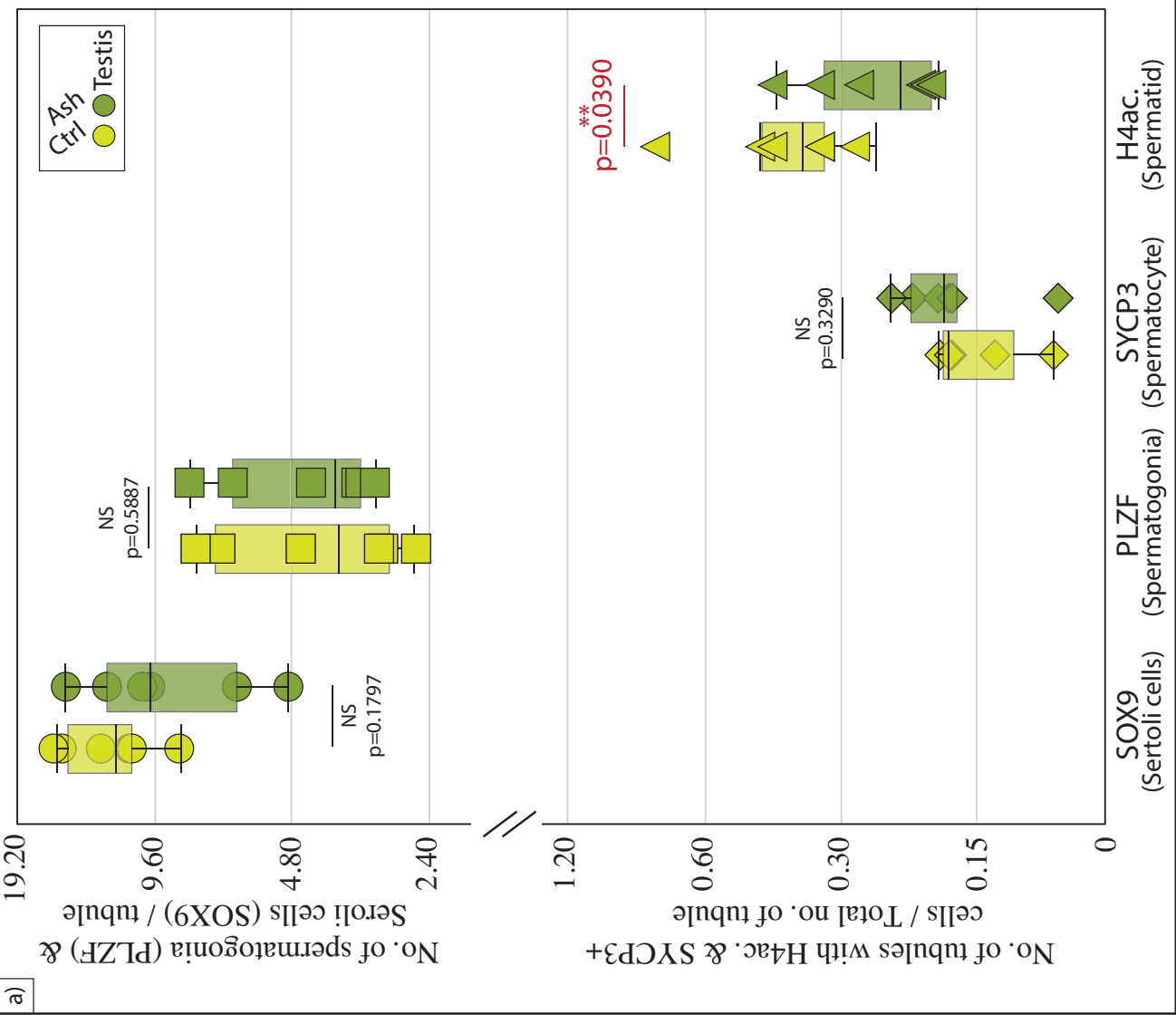


**Figure 6: Immunohistochemical quantification of seminiferous tubules**

(a) Number of normal seminiferous tubules of control and volcanic-ash exposed C57BL/6 males (n=6 per group). Statistical analysis: NS stand for non significant value, \*\* is for p<0.05 (two-sided non-parametric Mann-Whitney U-test implemented in MATLAB™) (b) & (c) Correlation between the testicular Fe and Cu concentration and the number of acetyl H4+ tubules versus the total number of tubules (n>20). Error bars represent 2sd.

Figure 7

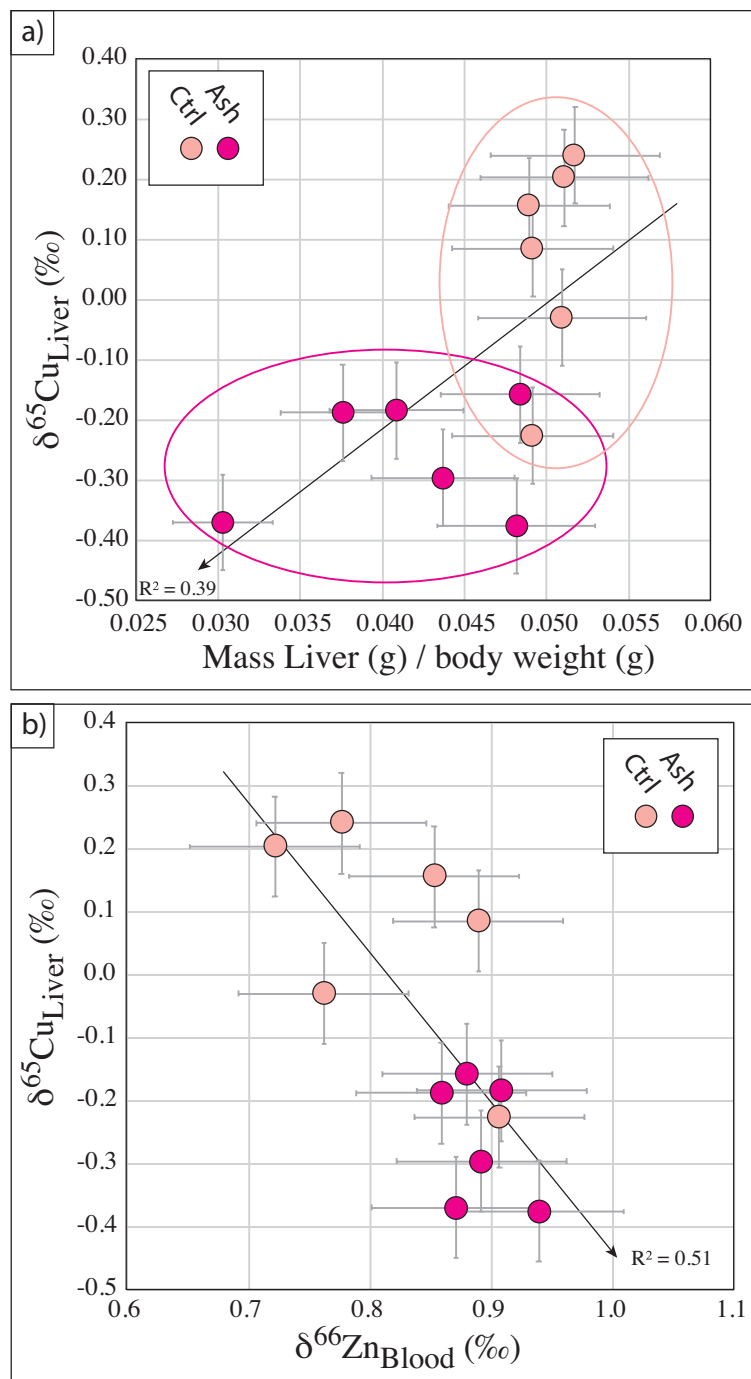


**Figure 7: Volcanic ash-related isotopic and physiological deregulations in liver and blood mice**

Mice exposed to volcanic ash present a significant decrease of the hepatic copper isotopic composition ( $\delta^{65}\text{Cu}$ ) in association with (a) a liver mass loss and (b) a rise of the blood zinc isotopic composition ( $\delta^{66}\text{Zn}$ ). Light and dark points stand for control and exposed subjects, respectively. For each value, analytical error bars represent 2sd.



Click here to access/download  
**Supplementary Material**  
Supp Table2.xlsx





Click here to access/download  
**Supplementary Material**  
Supp Table 1.xlsx





Click here to access/download  
**Supplementary Material**  
Supp Table3.xlsx





Click here to access/download  
**Supplementary Material**  
Supp Table4.xlsx







Click here to access/download  
**Supplementary Material**  
Supp Table5.xlsx





Click here to access/download  
**Supplementary Material**  
Supp Table6.xlsx






Click here to access/download  
**Supplementary Material**  
Supp Table7.xlsx



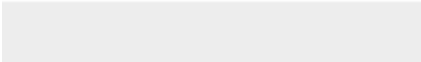



Click here to access/download  
**Supplementary Material**  
Supp Figure1.eps





Click here to access/download  
**Supplementary Material**  
Supp Figure2.eps





Click here to access/download  
**Supplementary Material**  
Supp Figure3.eps





Click here to access/download  
**Supplementary Material**  
Supp Figure4.eps







Click here to access/download  
**Supplementary Material**  
Supp Figure5.eps





Click here to access/download  
**Supplementary Material**  
Supp Figure6.eps



**Declaration of interests**

☒The authors declare that they have no known competing financial interests or personal relationships that could have appeared to influence the work reported in this paper.

☐The authors declare the following financial interests/personal relationships which may be considered as potential competing interests:

### **Sample CRediT author statement**

**Sauzéat Lucie**: Conceptualization, Methodology, Software, Validation, Investigation, Writing – Original draft, Review & Editing, Visualization, Supervision, Project administration, Funding acquisition;

**Julia Eychenne**: Writing – Review & Editing, Methodology, Investigation

**Lucia Gurioli**: Resources, Writing – Review & Editing

**Maud Boyet**: Supervision, Writing – Review & Editing

**David Jessop**: Resources, Writing – Review & Editing

**Roberto Moretti**: Resources, Writing – Review & Editing

**Mélusine Monroe**: Investigation

**Hélène Holota**: Investigation

**Claude Beaudoin**: Writing – Review & Editing

**David Volle**: Supervision, Methodology, Investigation, Writing – Review & Editing